Hailiang Mao | Moritaka Nakamura | Corrado Viotti | Markus Grebe

A Framework for Lateral Membrane Trafficking and Polar Tethering of the PEN3 ATP-Binding Cassette Transporter

Suggested citation referring to the original publication:
Plant Physiology 172 (2016) 4, 2245–2260
DOI https://doi.org/10.1104/pp.16.01252
ISSN (print) 0032-0889
ISSN (online) 1532-2548

A Framework for Lateral Membrane Trafficking and Polar Tethering of the PEN3 ATP-Binding Cassette Transporter[1][CC-BY]

Hailiang Mao, Moritaka Nakamura, Corrado Viotti, and Markus Grebe*

Umeå Plant Science Centre, Department of Plant Physiology, Umeå University, SE-90 187 Umeå, Sweden (H.M., M.G.); and Institute of Biochemistry and Biology, Plant Physiology, University of Potsdam, 14476 Potsdam-Golm, Germany (M.N., C.V., M.G.)

ORCID ID: 0000-0001-7571-0670 (M.G.).

The outermost cell layer of plants, the epidermis, and its outer (lateral) membrane domain facing the environment are continuously challenged by biotic and abiotic stresses. Therefore, the epidermis and the outer membrane domain provide important selective and protective barriers. However, only a small number of specifically outer membrane-localized proteins are known. Similarly, molecular mechanisms underlying the trafficking and the polar placement of outer membrane domain proteins require further exploration. Here, we demonstrate that ACTIN7 (ACT7) mediates trafficking of the PENETRATION3 (PEN3) outer membrane protein from the trans-Golgi network (TGN) to the plasma membrane in the root epidermis of Arabidopsis (*Arabidopsis thaliana*) and that actin function contributes to PEN3 endocytic recycling. In contrast to such generic ACT7-dependent trafficking from the TGN, the EXOCYST84b (EXO84b) tethering factor mediates PEN3 outer-membrane polarity. Moreover, precise EXO84b placement at the outer membrane domain itself requires ACT7 function. Hence, our results uncover spatially and mechanistically distinct requirements for ACT7 function during outer lateral membrane cargo trafficking and polarity establishment. They further identify an exocyst tethering complex mediator of outer lateral membrane cargo polarity.

Many cell types of diverse organisms display persistent, asymmetric distribution of molecules or structures along an axis. This phenomenon referred to as cell polarity often enables cells to fulfill specific functions. Cell polarity may be reflected by the asymmetric, polar localization of proteins to specific areas at the plasma membrane (PM). Much work has focused on polar localization of auxin transport facilitators of the PIN-FORMED (PIN) protein family in Arabidopsis (*Arabidopsis thaliana*; Gälweiler et al., 1998; Müller et al., 1998; Geldner et al., 2001; Wisniewska et al., 2006). For example, PIN2 marks the shootward-oriented (apical) PM domain of root epidermal cells, and the root tip-oriented (basal) domain of cortical cells in the root meristem (Blilou et al., 2005), while PIN1 marks the basal domain of root vascular cells (Steinmann et al., 1999). Thus, PIN2 and PIN1 highlight specific membrane domains along the apical-basal axis of specific cell types, and regulators of PIN1 activity and polarity have been identified (Geldner et al., 2003; Michniewicz et al., 2007). Mechanisms underlying PIN protein trafficking and targeting to specific domains have been addressed over the last two decades (Kleine-Vehn and Friml, 2008). Similarly, polar emergence of root hairs from a local area at the outer epidermal PM has been studied in detail (Grebe et al., 2002; Fischer et al., 2006; Ikeda et al., 2009; Kiefer et al., 2015). However, only more recently, proteins have become known that specifically localize broadly along the epidermal PM at the root surface facing the soil, termed the outer (lateral) membrane (Miwa et al., 2007; Strader and Bartel, 2009; Alassimone et al., 2010; Takano et al., 2010; Fendrych et al., 2013; Barberon et al., 2014). In line with a function of the outer lateral membrane as a target and selective barrier for inorganic and biotic compounds or stresses, proteins involved in biotic stress response or transport of abiotic compounds display polar localization at the outer domain. These include the ATP-binding cassette (ABC) transporter PENETRATION3 (PEN3)/PDR8/ABCG36 (Strader and Bartel, 2009), originally identified due to its function in response to penetrating fungal pathogens (Stein et al., 2006), and its close homolog ABCG37 (Łangowski et al., 2010, Ruzicka et al., 2010).

[1] This work was supported by the European Research Council starting (consolidator) grant ERC-STG-2010 Green-Lat-Pol (grant no. 260699 to M.G.).

* Address correspondence to markus.grebe@uni-potsdam.de.

The author responsible for distribution of materials integral to the findings presented in this article in accordance with the policy described in the Instructions for Authors (www.plantphysiol.org) is: Markus Grebe (markus.grebe@uni-potsdam.de).

M.G. conceived the project; M.G. and H.M. designed experiments; H.M., C.V., and M.N. performed experiments; M.G., H.M., M.N., and C.V. interpreted the results; M.G. and H.M. wrote the manuscript; all authors read and edited the manuscript prior to publication.

www.plantphysiol.org/cgi/doi/10.1104/pp.16.01252

Outer membrane proteins involved in ion/nutrient uptake include the IRON-REGULATED TRANSPORTER1 (IRT1; Barberon et al., 2014), the boron exporter BOR4 (Miwa et al., 2007), and the boric acid uptake channel NIP5;1 (Alassimone et al., 2010; Takano et al., 2010), and NIP5;1 subcellular localization depends on D-Gal (Uehara et al., 2014). Another boric acid/borate exporter, BOR1, localizes to the inner lateral membrane of root epidermal cells bordering the cortical cell layer, and specific Tyr residues in BOR1 mediate its polar localization and vacuolar targeting (Takano et al., 2010). With respect to IRT1, the phosphatidylinositol-3-phosphate-binding protein FYVE1 is required for IRT1 recycling and affects IRT1 polar delivery to the outer domain (Barberon et al., 2014). Trafficking of PEN3, ABCG37, and BOR4 proved sensitive to pharmacological interference with the actin cytoskeleton as well as chemical interference with secretory trafficking mediated by small ADP-ribosylation factor1 (ARF1)-type GTPases (Łangowski et al., 2010). Given the limited number of studies performed, mechanisms mediating trafficking and polarity of outer polar domain cargo still largely remain to be addressed. The last steps for a secretory vesicle carrying a transmembrane protein would be tethering, docking, and fusion with the target membrane during exocytosis. The tethering step may be facilitated by the exocyst tethering complex, a conserved octameric protein complex in eukaryotes (Heider and Munson, 2012). Components of the exocyst complex, including EXO84b, EXO70A1, and others, are polarly localized at the outer lateral membrane of Arabidopsis root epidermal cells (Fendrych et al., 2013). However, their functions in establishment of outer membrane cargo polarity remain to be further explored. Here, we examine mechanisms underlying PEN3 trafficking to and its polar localization at the outer lateral membrane domain.

RESULTS

PEN3 Endocytosis from and Recycling to the Outer Lateral Membrane

In contrast to apical and basal membrane cargos that largely rely on endocytic trafficking or recycling for their polarity establishment (Geldner et al., 2001; Geldner et al., 2003), polar delivery to the outer membrane domain in the root epidermis has been suggested to be mainly mediated by polar secretion (Łangowski et al., 2010). This interpretation is based on treatment of Arabidopsis seedlings with the vesicle trafficking inhibitor brefeldin A (BFA; Łangowski et al., 2010). BFA targets guanine nucleotide exchange factors that regulate the activity of ARF-type small GTPases (Steinmann et al., 1999; Robineau et al., 2000; Geldner et al., 2003). BFA action may affect the secretory and/or endocytic recycling pathway, depending on the BFA sensitivity of a given ARF guanine nucleotide exchange factor expressed in a specific tissue and its respective action in a given trafficking pathway (Richter et al., 2007). Compared to control cells treated with dimethyl sulfoxide (DMSO) solvent only (Fig. 1A), a functional PEN3-GFP fusion (PEN3-GFP) expressed from its own promoter (Stein et al., 2006), accumulated in endomembrane agglomerations (so-called BFA compartments or BFA bodies) upon BFA treatment, while PEN3-GFP polarity was not affected in epidermal cells (Fig. 1B), consistent with previous observations (Łangowski et al., 2010). After pretreating seedlings with the protein translation inhibitor cycloheximide (CHX) followed by cotreatment with CHX and BFA, we found that this reduced the size and fluorescence intensity of PEN3-GFP-labeled BFA compartments (Fig. 1, C and D). However, quantitative and statistical analyses revealed that a significant number of BFA compartments remained despite CHX cotreatment (Fig. 1, I–K; Supplemental Tables S1 and S2). We confirmed that CHX treatment targeted translation of PEN3-GFP cargo contributing to secretory trafficking (see below). Our findings indicate that in addition to the secretory pathway that we find contributes to PEN3-GFP accumulation in BFA compartments as previously highlighted (Łangowski et al., 2010), other trafficking pathways such as endocytic trafficking may be involved as well.

To address a potential contribution of endocytosis, we applied the endocytosis inhibitor Wortmannin (Wm) which targets phosphoinositide kinases (Volinia et al., 1995; Emans et al., 2002; Jaillais et al., 2006). When compared to BFA treatment only (Fig. 1B), Wm pretreatment followed by combined Wm and BFA treatment efficiently inhibited PEN3-GFP accumulation in BFA compartments (Fig. 1, E and F, arrowheads in F), as investigated by quantitative and statistical analyses of the number of BFA bodies per root, the area size of BFA compartments, and their relative signal intensity (Fig. 1, I–K; Supplemental Tables S1 and S2). When using combined application of Wm and CHX pretreatment followed by Wm, CHX, and BFA, BFA compartment formation was even further reduced (Fig. 1, G–K; Supplemental Tables S1 and S2). These findings indicated a contribution of both the secretory and the endocytic pathways to PEN3 accumulation in BFA compartments.

To more directly monitor PEN3 endocytosis and recycling, we generated plants expressing PEN3 fused to the green-to-red photoconvertible fluorescent protein mEos2 (McKinney et al., 2009) under the control of the *PEN3* promoter (*pPEN3:PEN3-mEos2*; Fig. 2A). The PEN3-mEos2 fusion protein proved to be functional, restoring the long-root-hair phenotype of the *pen3-4* mutant to wild-type levels (Supplemental Fig. S1, A and B). Similarly, we generated a functional *pPEN3:PEN3-mCherry* in *pen3-4*, which reduced the root hair length of the *pen3-4* mutant even somewhat below wild-type levels (Supplemental Fig. S1, B and C). The subcellular distribution of PEN3-mCherry in root epidermal cells was indistinguishable from functional PEN3-GFP (Supplemental Fig. S1D) described previously (Stein et al., 2006). In order to track PEN3 endocytosis, we photoconverted PEN3-mEos2 at a selected PM region (Fig. 2, A and B) and monitored its trafficking in presence of BFA. Within 34 min after BFA treatment, the photoconverted red form of PEN3-mEos2 (PEN3-mEos2-R; magenta, Fig. 2C, middle) accumulated inside BFA

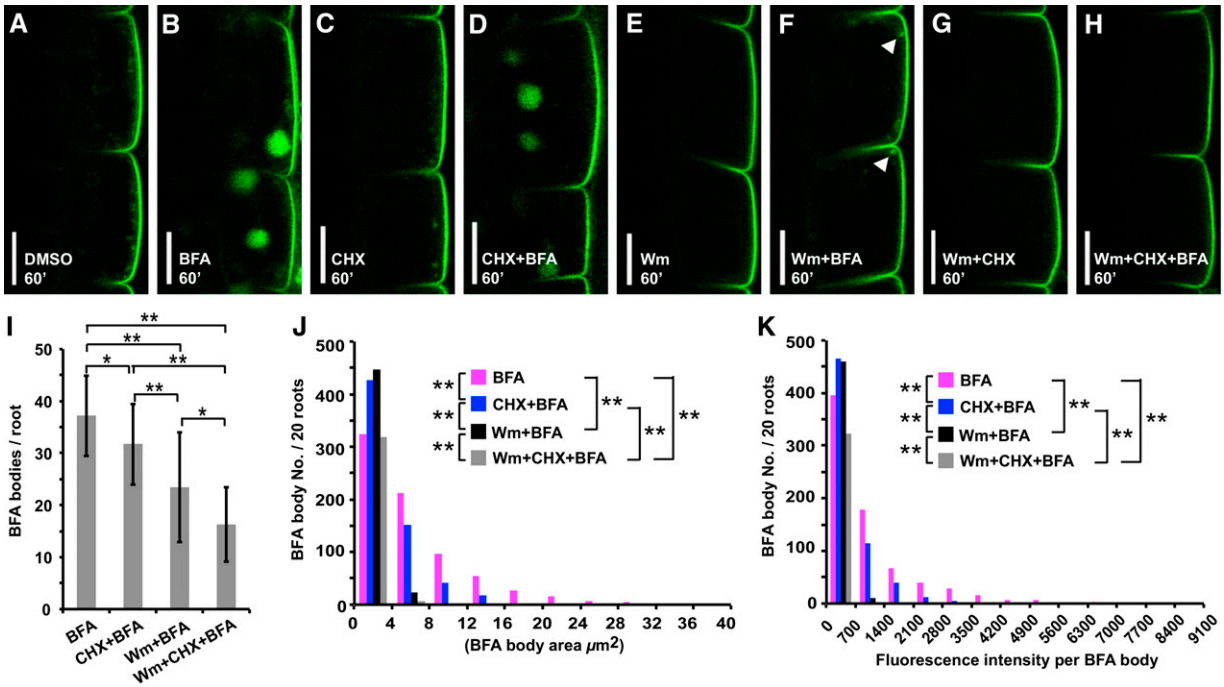

Figure 1. Pharmacological interference indicates contributions of secretory and endocytic pathways to PEN3 trafficking. A to H, Root epidermal cells of 5-d-old Arabidopsis seedlings expressing PEN3-GFP treated with (A) 60 min 0.2% DMSO, (B) 60 min 50 μM BFA, (C) 60 min 50 μM CHX, (D) 60 min 50 μM CHX pretreatment followed by 60 min 50 μM CHX, 50 μM BFA, (E) 60 min 33 μM Wm, (F) 60 min 33 μM Wm pretreatment followed by 60 min 33 μM Wm, 50 μM BFA, (G) 60 min 33 μM Wm, 50 μM CHX, (H) 60 min 33 μM Wm, 50 μM CHX pretreatment followed by 60 min 33 μM Wm, 50 μM CHX, 50 μM BFA. I to K, Quantitative and statistical analysis of (I) BFA bodies per root, (J) BFA body size, (K) fluorescence intensity per BFA body from experiments such as B, D, F, and H from one midplane optical CLSM section of $n = 20$ roots per condition. Images were acquired between 60 ± 5 min after BFA application (60'). Note, very small BFA bodies in F (arrowheads) and no BFA body in H. I, Student's two-tailed t test with equal variance was used to detect significances of differences between average number of BFA bodies from $n = 20$ roots per treatment. $^{**}P < 0.01$. $^{*}P < 0.05$. Exact P values are shown in Supplemental Table S1. Statistical differences of BFA body size (J) and fluorescence intensity per BFA body (K) between treatments were determined by nonparametric, two-sample KS test. $^{**}P = 0.000$. Exact P values are shown in Supplemental Table S2. Total numbers of BFA bodies analyzed were (B) $n = 743$ for BFA treatment, (D) $n = 639$ for CHX and BFA treatment, (G) $n = 470$ for Wm and BFA treatment, (H) $n = 326$ for Wm, CHX, and BFA treatment. Bars = 10 μm.

compartments together with the green form (green, Fig. 2C, left). We quantified the fluorescence intensity of photoconverted PEN3-mEos2 both at the PM and in BFA compartments. After photoconversion, PEN3-mEos2-R intensity was significantly increased at the PM (Fig. 2D). PEN3-mEos2-R strongly accumulated inside BFA compartments monitored at 30 ± 4 min after BFA application, when compared to the time point directly after photoconversion (Fig. 2E), while the PEN3-mEos2-R intensity at the PM was significantly decreased at 30 ± 4 min, demonstrating endocytosis of red-fluorescent PEN3-mEos2 from the outer lateral PM (Fig. 2, D and E). To test for potential recycling, we treated seedlings with BFA to accumulate PEN3-mEos2 in BFA compartments, then washed out BFA and, immediately after washout, photoconverted PEN3-mEos2 localized in BFA compartments (Fig. 2, F and G). Strikingly, we observed a reaccumulation of red-fluorescent PEN3-mEos2 at the outer lateral PM (Fig. 2, H and I), although the fluorescence intensity decreased again after 60 min (Fig. 2I), probably due to endocytosis and/or additional photobleaching. Taken together, our findings strongly suggest that PEN3 is endocytosed from and recycled back to the outer lateral PM domain.

PEN3 Endocytic and Secretory Trafficking via the trans-Golgi Network

In addition to its polar localization at the outer lateral PM, PEN3-GFP accumulated in intracellular membrane compartments (Fig. 3, A and B). Biochemical copurification experiments of PEN3 with the TGN-localized SYP61 syntaxin suggest that these intracellular compartments include TGN membranes (Drakakaki et al., 2012). To investigate whether PEN3 localizes to the TGN in vivo, we generated transgenic plants coexpressing PEN3-GFP and the TGN markers VHA-a1-mRFP (Dettmer et al., 2006) or Vti12-mCherry/WAVE13R (Geldner et al., 2009). Indeed, cytoplasmic PEN3-GFP colocalized with both

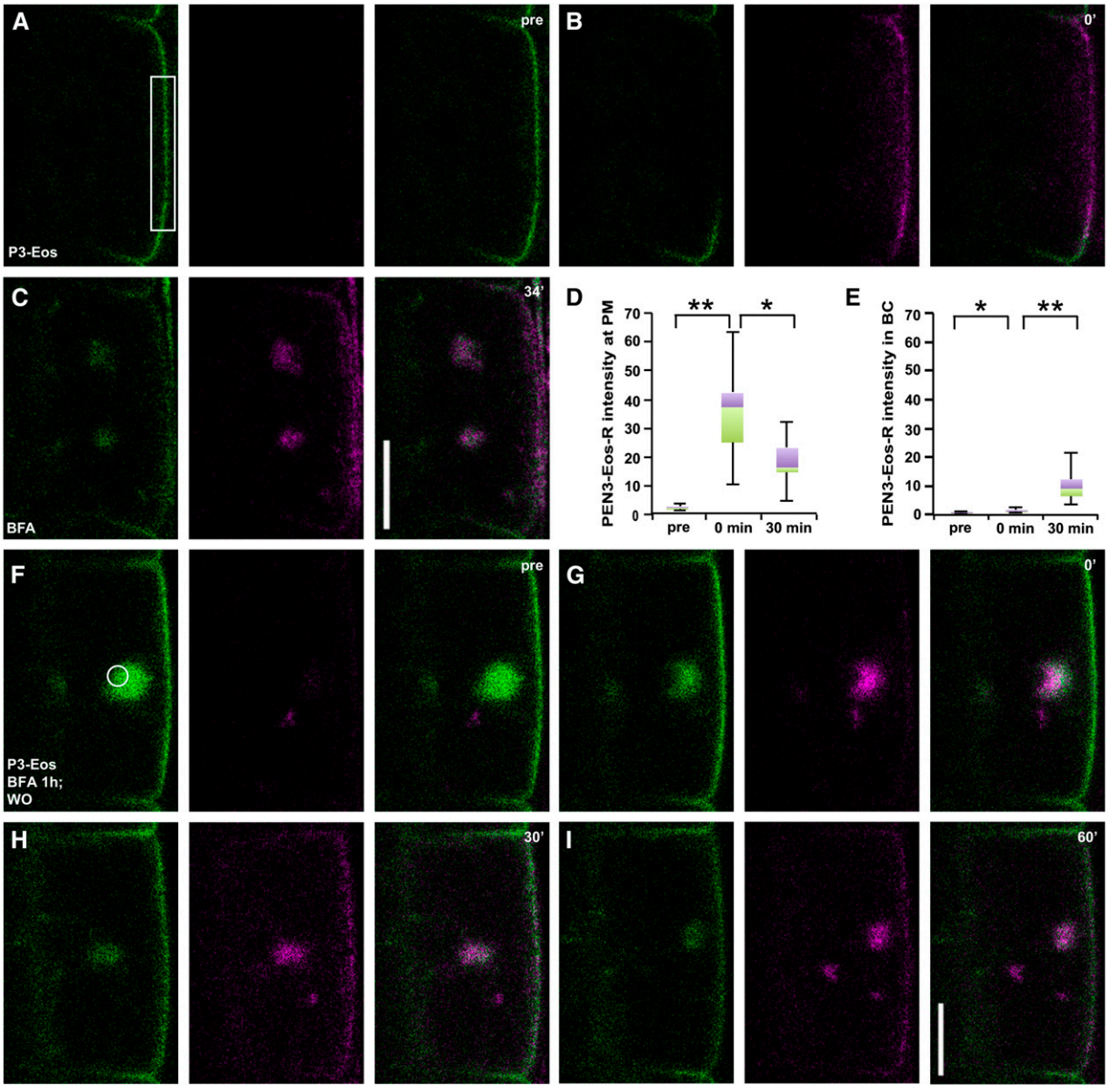

Figure 2. PEN3-mEos2 endocytosis from and recycling to the outer lateral membrane. A to E, PEN3-mEos2 (P3-Eos) internalization from the outer lateral domain into BFA bodies after green-to-red photoconversion in the indicated ROI frame. A to C, PEN3-mEos2 treated with 50 μM BFA after photoconversion. Time points (A) prior to (pre) photoconversion, (B) after photoconversion (0′), and (C) after application of 50 μM BFA (34′) are indicated. D and E, Quantitative and statistical analysis of photoconverted PEN3-mEos2 (PEN3-Eos-R) intensity at (D) the PM or (E) in BFA compartments (BC). Box-and-whiskers plots are displayed for n = 10 cells prior to photoconversion (pre), directly after photoconversion (0 min), and 30 min after photoconversion. Whiskers indicate maximum and minimum values of the population. Violet boxes, 25% of values above median. Green boxes, 25% of values below median. Data are derived from CLSM images such as in A to C. Images at 30 min were acquired between 29 and 34 min after BFA application. Statistical differences were determined by two-tailed, type 1 paired t test with n = 10 cells (from seven roots). D, $^{**}P = 0.000$ pre versus 0 min; $^{*}P = 0.003$ 0 min versus 30 min. E, $^{*}P = 0.001$ pre versus 0 min; $^{**}P = 0.000$ 0 min versus 30 min. F to I, PEN3-mEos2 recycling from a BFA body to the outer lateral PM after photoconversion. After 60 min of 50 μM BFA pretreatment followed by BFA washout, photoconversion was conducted between pre (F) and 0′ (G) after BFA washout. PEN3-mEos2 redistribution monitored at indicated time points after BFA washout. n = 17 cells (from 15 roots) were observed with similar results. Bars = 10 μm.

VHA-a1-mRFP (Fig. 3A) as well as Vti12-mCherry/WAVE13R (Fig. 3B). Quantitative colocalization analyses of the geometrical centers of compartments labeled in two different channels, revealed 46% of intracellular PEN3-GFP to colocalize with VHA-a1-mRFP and 50% with Vti12-mCherry/WAVE13R (Fig. 3C). We also coexpressed PEN3-GFP with SYP61-CFP (Robert et al., 2008) and the cis-Golgi marker SYP32-mCherry/

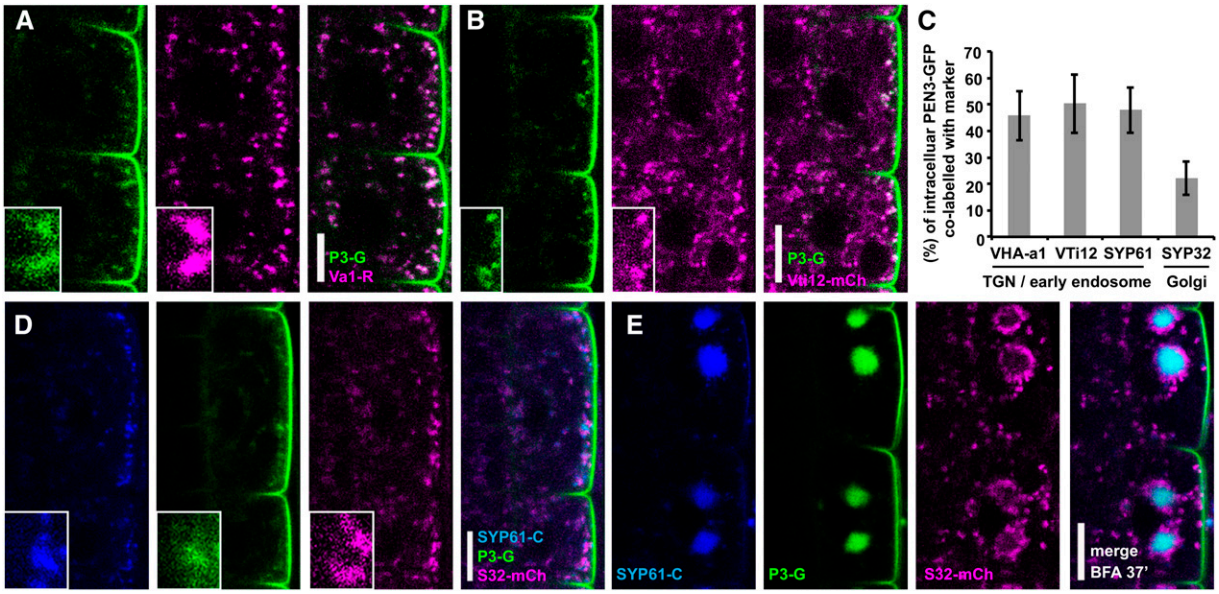

Figure 3. Cytoplasmic PEN3 preferentially colocalizes with trans-Golgi network markers. A and B, CLSM colocalization analyses in root epidermal cells of 5-d-old seedlings (A) coexpressing PEN3-GFP (P3-G, green) with VHA-a1-mRFP (Va1-R, magenta), and (B) with VTI12-mCherry/WAVE13R (Vti12-mCh, magenta). C, Quantitative colocalization analysis given as the percentage (%) of intracellular PEN3-GFP colabeled with marker compartments. Data are derived from CLSM images such as in A, B, and D with averages ± SD given for $n = 15$ cells per marker. D and E, Colocalization analysis of TGN marker SYP61-CFP (SYP61-C, blue), PEN3-GFP (green), and Golgi marker SYP32-mCherry/WAVE22R (S32-mCh, magenta) (D) after 37 min of 0.1% DMSO and (E) 37 min 50 μM BFA. Bars = 10 μm.

WAVE22R (Geldner et al., 2009). Strikingly, PEN3-GFP fluorescence in endomembrane compartments overlapped with SYP61-CFP but was regularly flanked only by the SYP32-mCherry/WAVE22R signal (Fig. 3D). This became even more evident after BFA treatment, when PEN3-GFP and SYP61-CFP strongly coaggregated in the core of BFA bodies, which was surrounded by SYP32-mCherry/WAVE22R-labeled Golgi bodies (Fig. 3E). These observations were highly similar to the previously reported agglomeration of TGN-derived material in the core of BFA compartments and the positioning of Golgi stacks at the periphery of BFA compartments (Grebe et al., 2003; Geldner et al., 2003). Quantitative analysis of nontreated cells showed that 48% of intracellular PEN3-GFP colocalized with SYP61-CFP compared to 22% colocalizing with SYP32-mCherry/WAVE22R (Fig. 3C). Our results demonstrate that PEN3-GFP preferentially localizes to TGN compartments, providing in vivo support for previous biochemical membrane isolation studies (Drakakaki et al., 2012).

In light of PEN3-GFP localization to the TGN, we investigated whether PEN3 secretory and/or endocytic trafficking occurred via this intracellular sorting hub. About 4 min after application of the widely used endocytic tracer FM4-64 (Vida and Emr, 1995), we observed PEN3-GFP colocalization with FM4-64 (Fig. 4A). Such rapidly FM4-64-labeled membranes have previously been identified as VHA-a1-positive TGN/early endosomal compartments (Dettmer et al., 2006). After BFA treatment, PEN3-GFP and FM4-64 coaggregated in the core of BFA compartments (Fig. 4B). These findings strongly support that PEN3 traverses a TGN compartment involved in early endocytic trafficking. We next tested the effect of concanamycin A (ConcA), a specific inhibitor of V-ATPase that can block secretory and endocytic trafficking at the TGN (Dröse et al., 1993; Dettmer et al., 2006). After ConcA treatment, PEN3-GFP formed intracellular agglomerations, most of which overlapped with VHA-a1-mRFP (Fig. 4C), indicating that ConcA blocked PEN3-GFP at the TGN. Strikingly, CHX cotreatment greatly reduced PEN3-GFP, in the ConcA-induced agglomerations (Fig. 4, D–G), indicating that most PEN3-GFP in these agglomerations was derived from de novo-synthesized protein. VHA-a1-mRFP was less affected (Fig. 4, D–G), most likely, because it prevalently resides at the TGN at steady state. Similarly, outer lateral membrane localization of PEN3-GFP appeared unaffected (Fig. 4D). These findings confirmed efficient CHX action on PEN3-GFP synthesis. Together, our results strongly suggest that both endocytic and secretory trafficking contribute to PEN3 aggregation in BFA-induced compartments as well as to its localization at the TGN.

ACT7 Mediates TGN-PM Trafficking of Outer Lateral Membrane Cargo

To investigate potential cytoskeletal requirements of PEN3 trafficking to and from the TGN, we applied inhibitors affecting microtubule (MT) or actin organization.

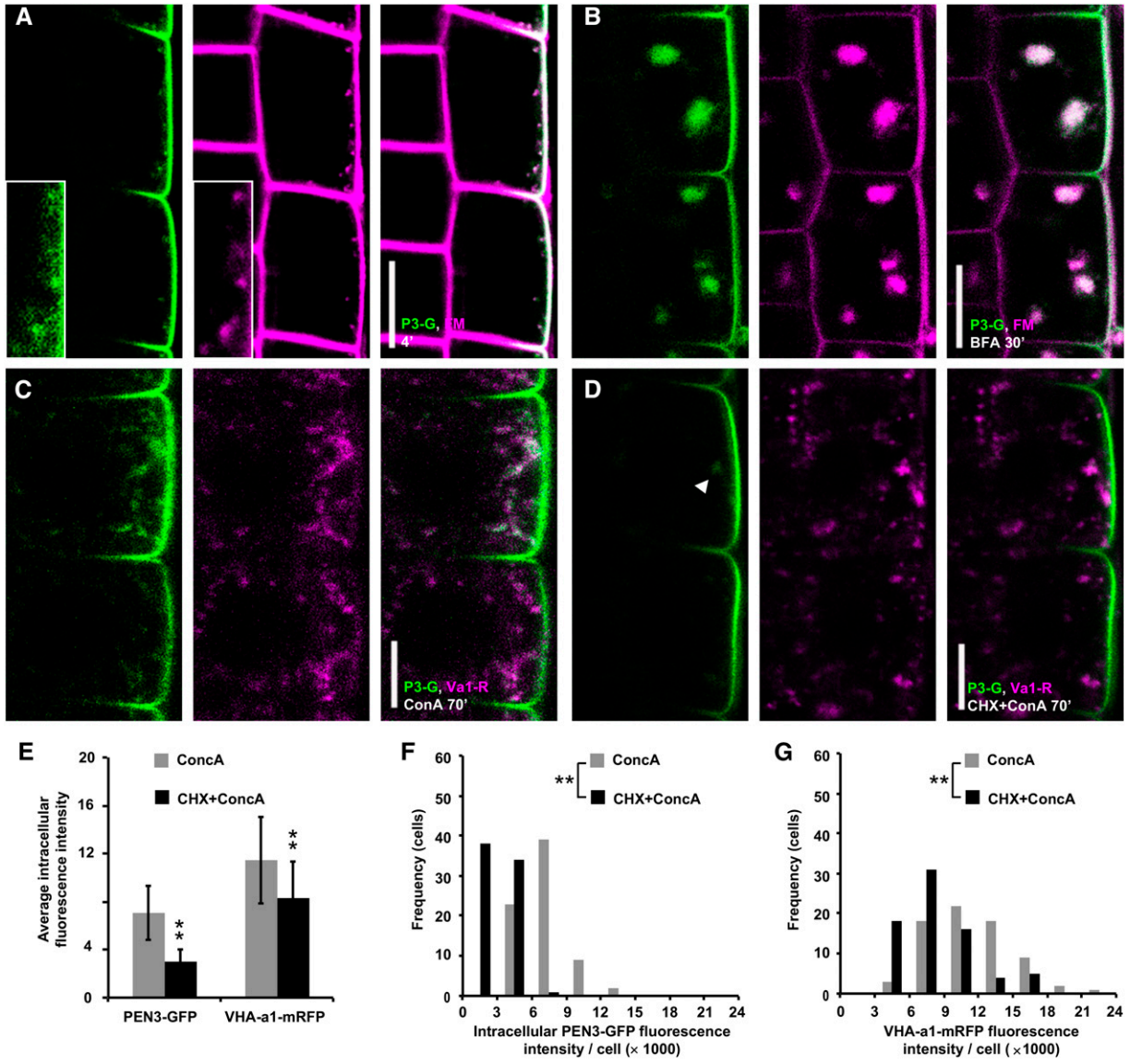

Figure 4. PEN3 endocytic and secretory trafficking via the trans-Golgi network. A, Untreated cells expressing PEN3-GFP (P3-G, green) labeled with FM4-64 (FM, magenta) for 4 min. B, Cells expressing PEN3-GFP treated with BFA for 30 min in presence of FM4-64. Images at 30 min were acquired between 27 and 32 min after BFA application. $n = 9$ independent roots analyzed with similar results. C, Cells coexpressing PEN3-GFP (P3-G, green) and VHA-a1-mRFP (Va1-R, magenta) treated for 70 min with 2 μM ConcA. D, Cells coexpressing PEN3-GFP (P3-G, green) and VHA-a1-mRFP (Va1-R, magenta) pretreated 45 min 50 μM CHX followed by 70 min 2 μM ConcA, 50 μM CHX. Images at 70 min were acquired between 65 and 75 min after ConcA application. E to G, Quantitative and statistical analysis of average intracellular fluorescence intensity per cell of PEN3-GFP (E and F) and for (E and G) VHA-a1-mRFP from experiments such as in C and D from one midplane CLSM section per root. $n = 73$ cells from 10 roots per treatment. Statistical differences were determined by nonparametric, two-sample KS test. $^{**}P = 0.000$. Bars = 10 μm.

Consistent with previous observations (Łangowski et al., 2010), the MT-depolymerizing drug oryzalin affected neither PEN3-GFP polar localization nor its intracellular distribution after a 2-h treatment that, however, resulted in cortical MT depolymerization (Supplemental Fig. S2, A and B). These results are also in agreement with data showing that relocalization of PEN3-GFP to pathogen penetration sites does not depend on MTs (Underwood and Somerville, 2013).

In comparison, the actin depolymerizing drug latrunculin B (LatB) induced PEN3-GFP agglomeration in endomembrane compartments without exerting visible defects on PEN3 outer membrane polarity (Fig. 5, A–H; Łangowski et al., 2010). Strikingly, we observed that these compartments colabeled with PEN3-GFP and the endocytic tracer FM4-64 as early as 5 min after uptake, suggesting that FM4-64 endocytosis remained largely unaffected in presence of LatB (Fig. 5, A–H). In

presence of LatB, internalized FM4-64 was arrested in these agglomerations 1 h after its application and did not reach the tonoplast membrane, which at the same time started to be labeled in DMSO-treated control roots (Fig. 5, D and H). These results suggest that LatB at the concentrations employed does not largely inhibit endocytosis but may more strongly interfere at an early step of endocytic trafficking and/or recycling.

We next tested whether LatB affected endocytic recycling of PEN3-mEos2. Upon BFA washout with medium containing LatB, we observed a weak reconstitution of photoconverted red PEN3-mEos2 at the outer lateral PM (Fig. 5, I to L). In order to quantitatively address a potential effect of LatB on PEN3 recycling, we quantified and compared the experiments of BFA treatment and BFA washout in presence or absence of LatB, respectively, as shown in Figure 2, F to I. LatB significantly inhibited photoconverted PEN3-mEos2 accumulation at the outer lateral PM from BFA compartments, most notably at 30 min after BFA washout, when compared to BFA washout experiments in absence of LatB (Fig. 5M). The difference decreased 60 min after BFA washout (Fig. 5M), potentially due to continuous endocytosis and/or photobleaching. Our findings suggest that functional F-actin contributes to PEN3 recycling to the outer lateral PM domain.

The view that balanced F-actin function may be required for the regulation of PEN3 membrane trafficking

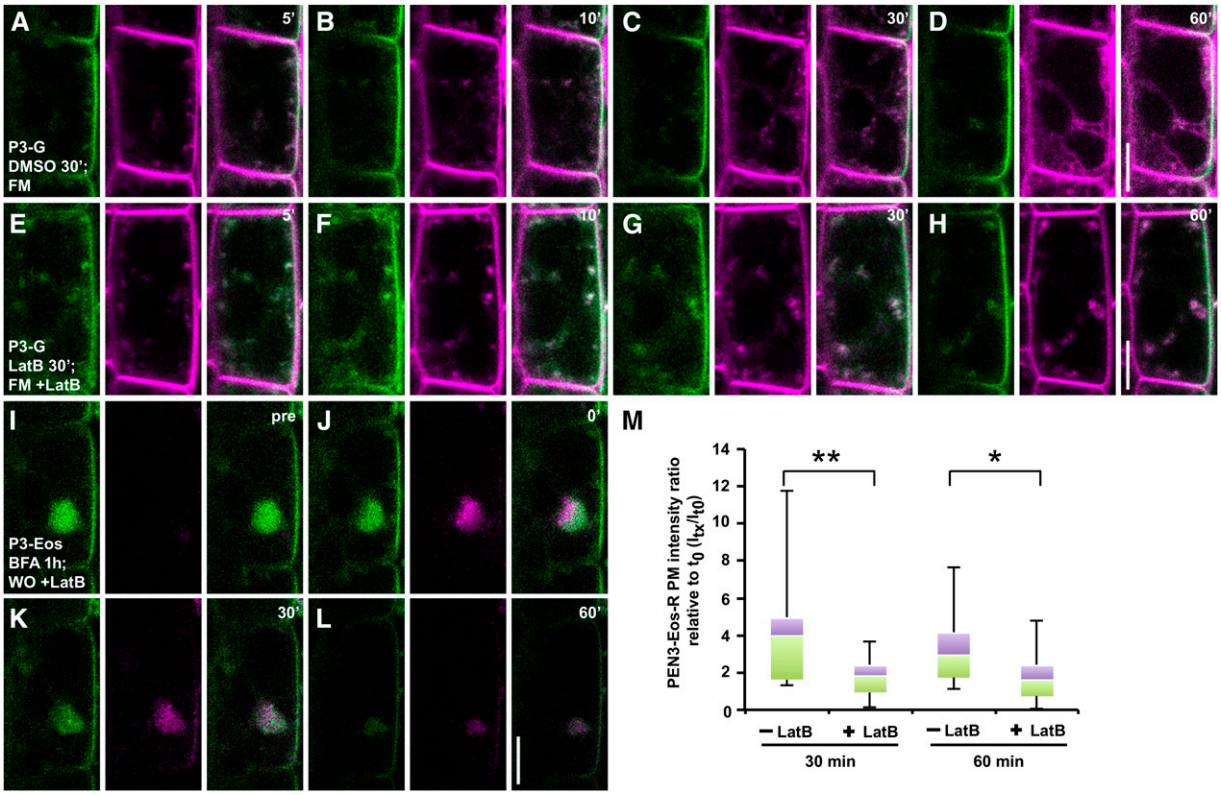

Figure 5. F-actin contributes to PEN3 endocytic trafficking and recycling. A to L, Root epidermal cells of 5-d-old seedlings. A to D, Cells expressing PEN3-GFP (P3-G, green) pretreated 30 min 0.1% DMSO, followed by 25 μM FM4-64 (FM, magenta) and two washes. E to H, Cells expressing PEN3-GFP pretreatment 30 min 10 μM LatB, followed by 25 μM FM4-64 and two washes in presence of 10 μM LatB (+LatB). Time points after washes are indicated. $n = 7$ independent roots analyzed with similar results. I to L, PEN3-mEos2 recycling from a BFA body to the outer lateral PM after photoconversion. After 60 min of 50 μM BFA pretreatment followed by BFA washout in presence of 10 μM LatB, photoconversion was conducted. I, Prior to photoconversion (pre). J, Immediately after photoconversion (0'). PEN3-mEos2 redistribution monitored at indicated time points after BFA washout. n = 17 cells (from 14 roots) were observed. M, Statistical analysis of red fluorescent photoconverted PEN3-mEos2 (PEN3-Eos-R) relative intensity redistribution at the outer lateral PM domain after 30 min and 60 min BFA washout in presence or absence of LatB (−LatB or +LatB), respectively. Intensity of PEN3-Eos-R fluorescence at PM after 30 min or 60 min BFA washout (I_{tx}) divided by the respective PM intensity immediately after photoconversion (I_{t0}) is presented as PEN3-Eos-R PM intensity ratio relative to t0 (I_{tx}/I_{t0}). Box-and-whiskers plots are displayed for $n = 17$ cells. Whiskers indicate maximum and minimum values. Violet boxes, 25% of values above median. Green boxes, 25% of values below median. Data are derived from CLSM images such as in I to L for +LatB or Figure 2, F to I, for the −LatB control. Statistical differences between I_{tx}/I_{t0} ratios at different time points were determined by two-tailed, unpaired t test with equal variance. $^{**}P = 0.003$ −LatB versus +LatB at 30 min; $^{*}P = 0.019$ −LatB versus +LatB at 60 min. Bars = 10 μm.

was further supported by the effects exerted by the actin stabilizing drug jasplakinolide (Jas). Jas treatment induced an accumulation of strong fragmented bundles of F-actin accompanied by PEN3-mCherry agglomeration in intracellular compartments without exerting obvious effects on PEN3 outer membrane polarity (Supplemental Fig. S2, C–F).

To identify the actin isoform involved, we examined PEN3-GFP distribution in the *actin2-3* (*act2-3*) loss-of-function mutant, defective in root-hair tip growth (Nishimura et al., 2003). However, we did not observe a deviation from PEN3-GFP wild-type localization in *act2-3* (Supplemental Fig. S3A). Nevertheless, we obtained genetic evidence for the actin isoform involved from a fluorescence microscopy-based genetic screen for PEN3-GFP mislocalization in roots of 5-d-old M2 seedlings from an ethyl methanesulfonate-mutagenized population. We identified three mutant lines that displayed large intracellular PEN3-GFP aggregations in dividing and early elongating cells (Fig. 6, A and B; Supplemental Fig. S3B). The overall seedling phenotype of these mutants resembled the one of *act7-6* and *act7-7* mutants recently characterized for root-hair positioning defects (Kiefer et al., 2015). Allelism tests with *act7-6* revealed noncomplementation of the PEN3-GFP agglomeration phenotype in the F1 generation (Fig. 6, A, C, and D). Similarly, *act7-7* revealed a PEN3-GFP mislocalization phenotype indistinguishable from *act7-6* and from the three newly isolated lines, which we named *act7-8*, *act7-9*, and *act7-10* (Fig. 6, A–C; Supplemental Fig. S3C). Sequencing of the *ACT7* genomic region revealed a point mutation in *act7-8* resulting in a C-to-T exchange altering Thr-108 (ACA) to Ile-108 (ATA), a G-to-A exchange resulting in a replacement of Gly-15 (GGA) by Glu-15 (GAA) in *act7-9*, while a G-to-A exchange caused a premature stop codon by replacement of Trp-81 (TGG) with TGA in *act7-10*. Hence, characterization of PEN3-GFP localization in three newly isolated and two previously described *act7* alleles revealed a strong contribution of ACT7 function to PEN3 trafficking. In addition, a highly similar mislocalization of the outer membrane protein NIP5;1-mCherry, as well as the nonpolar PM protein NPSN12/WAVE131R, were observed in *act7-6* (Fig. 6, E and F; Supplemental Figure S3, D and E). Similarly, PIN-family and ABCB-type auxin transporters, but not lateral membrane proteins, were recently shown to be mislocalized in the *act7-4 allele* (Zhu et al., 2016). Taken together, these results suggest a strong and general requirement of ACT7 function for nonpolar and polar transmembrane protein trafficking to diverse PM domains including the outer lateral domain.

In order to find out in which subcellular compartments PEN3-GFP might accumulate in *act7* mutants, we generated *act7-6* lines coexpressing PEN3-GFP with SYP32-mCherry/WAVE22R or VHA-a1-mRFP. Strikingly, the large PEN3-GFP aggregates in *act7-6* colocalized with VHA-a1-mRFP, while SYP32-mCherry/WAVE22R surrounded these PEN3-GFP agglomerations, which we coined *act7* compartments (Fig. 6, G and H). These agglomerations were clearly labeled by FM4-64 within 10 min after application, suggesting that arrest of FM4-64 trafficking occurred at an early step of an endocytic and/or recycling pathway in *act7-6* mutants (Figs. 5, A–H, and 6, I–L). When we specifically photoconverted PEN3-mEos2 in these *act7-6* compartments, the photoconverted red-fluorescent form of PEN3-mEos2 did not translocate to the PM even 1 h after photoconversion (Fig. 6, M–P). Quantitative analysis confirmed that no significant increase of red PEN3-mEos2 fluorescence above background was observed at the outer lateral PM (Fig. 6, Q–R). The decrease of red PEN3-mEos2 signal in *act7-6* compartments observed 30 min and 60 min after photoconversion might thus result from degradation and/or photobleaching (Fig. 6R), but certainly not from recycling to the PM. These results strongly support that ACT7 mediates PEN3 trafficking and likely its recycling from the TGN to the PM.

When analyzing the *act7-6* mutant by high-pressure freezing/freeze substitution followed by transmission electron microscopy, we observed large vesicle agglomerations that strongly resembled TGN-derived vesicles with peripherally associated Golgi stacks (Fig. 6S). In contrast to Golgi bodies displaying tubular and vesicular structures associated with the transmost Golgi cisternae in the wild type (Fig. 6T, arrowhead), *act7-6* mutants showed large vesicle accumulations directly starting at the transmost Golgi cisternae (Fig. 6U, arrowhead). Together, our findings suggest a preferential block of PEN3 at the TGN in *act7* mutants that display large aggregations of TGN-derived vesicles, which in part contribute to endocytic trafficking from and recycling to the outer lateral membrane.

EXO84b Mediates Polar Cargo Localization at the Outer Lateral Membrane

Exocyst complex components have been shown to be polarly localized at the outer lateral membrane and to be required for localization of a component of the SNARE docking and fusion machinery (Fendrych et al., 2013). We, therefore, next asked whether the exocyst complex might be involved in setting up polar distribution of the PEN3 cargo protein at the outer lateral membrane. We initially found that EXO84b-GFP and PEN3-mCherry colocalize at the outer lateral domain of root epidermal cell (Fig. 7A). To test whether exocyst function may be required for PEN3 localization, we introduced PEN3-GFP into the *exo84b-1* mutant. Strikingly, PEN3-GFP localization and polarity were severely affected in *exo84b-1* mutants (Fig. 7, B and C), where cells displayed strong intracellular accumulation of PEN3 and in some cells PEN3 outer lateral PM polarity was absent (Fig. 7, B, C, and F–H), despite those cells still being viable (Supplemental Movies S1 and S2). Similar defects were observed with respect to NIP5;1-mCherry distribution and polarity in the *exo84b-1* mutant (Fig. 7, D and E).

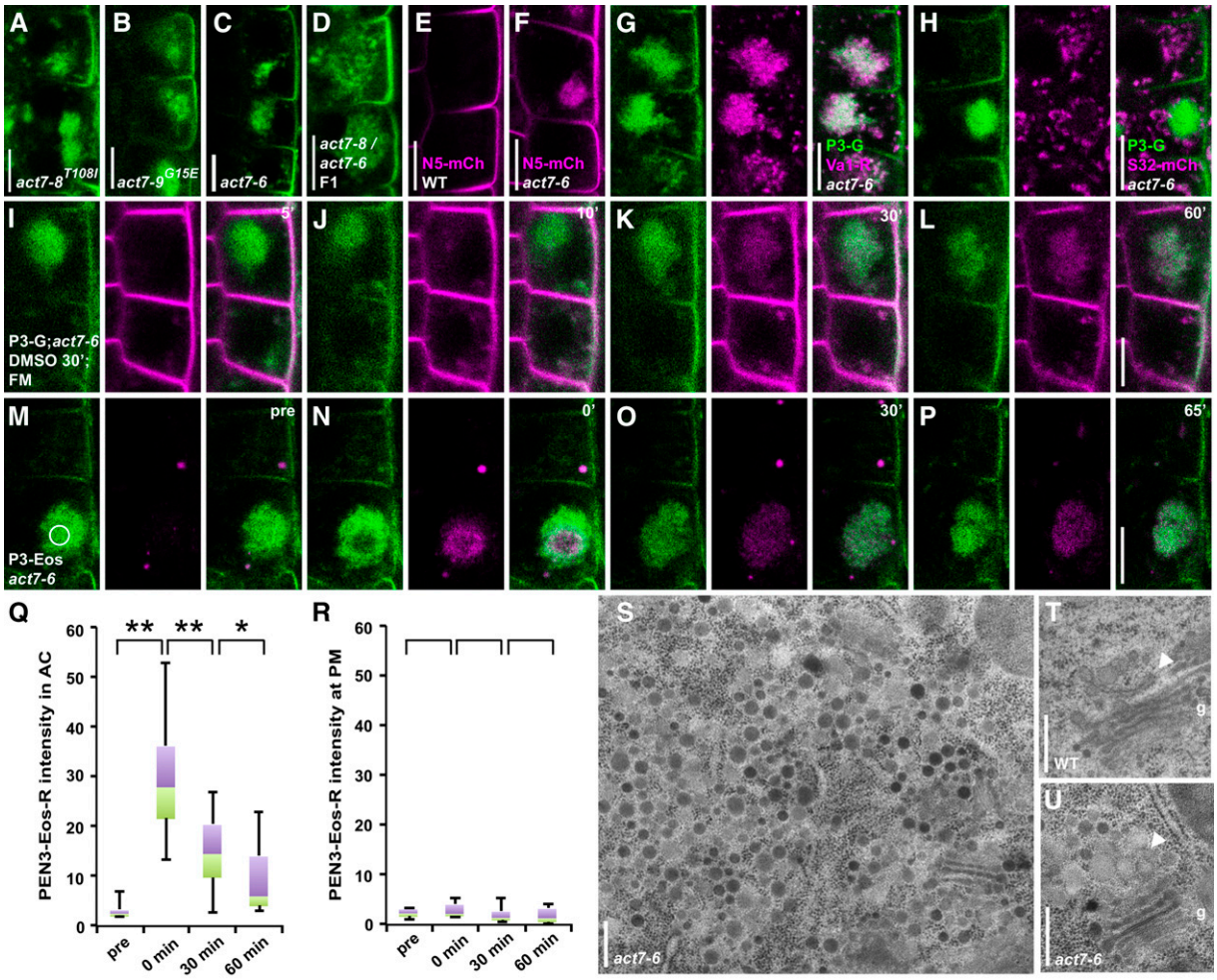

Figure 6. ACT7 mediates outer lateral membrane protein trafficking from the TGN. A to D, Subcellular PEN3-GFP localization in (A) *act7-8*, (B) *act 7-9*, (C) *act7-6*, and (D) *act7-6*/*act7-8* transheterozygote. E and F, NIP5;1-mCherry (N5-mCh) in (E) wild type and (F) *act7-6*. Note, large subcellular aggregations of PEN3-GFP in A to D and of NIP5;1-mCherry in F in *act7* mutants. G and H, PEN3-GFP coaggregation with (G) VHA-a1-mRFP (Va1-R) but not with (H) SYP32-mCherry/WAVE22R (S32-mCh) in *act7-6*. I to L, Pretreatment 30 min 0.1% DMSO followed by 25 μM FM4-64 (FM) and two washes. n = 7 independent roots observed with similar results. M to P, PEN3-mEos2 (P3-Eos) in *act7-6*. Distinct small dots of autofluorescence are visible (middle panel, right panel merge). Different time points after photoconversion to red (N) directly after (0′), (O) 30 min (30′), and (P) 65 min (65′) after photoconversion. Q and R, Quantitative and statistical analysis of photoconverted PEN3-mEos2 (PEN3-Eos-R) intensity (Q) in ACT7-compartments (AC) and (R) at the outer lateral PM. Box-and-whiskers plots are displayed for n = 10 cells prior to photoconversion (pre), directly after photoconversion (0 min), 30 min and 60 min after photoconversion. Whiskers indicate maximum and minimum values. Violet boxes, 25% of values above median. Green boxes, 25% of values below median. Images at 30 min acquired between 30 and 32 min after photoconversion. Images at 60 min acquired between 60 and 65 min after photoconversion. Data were derived from CLSM images such as in M to P. n = 10 cells from nine independent roots analyzed. Statistical differences were determined by two-tailed, type one paired t test. Q, $^{**}P$ = 0.000 pre versus 0 min; $^{**}P$ = 0.002 0 min versus 30 min; $^{*}P$ = 0.037 30 min versus 60 min. R, P = 0.111 pre versus 0 min; P = 0.121 0 min versus 30 min; P = 0.935 30 min versus 60 min. S to U, Ultrastructural analysis of intracellular vesicle aggregate in *act7-6* surrounded by Golgi stacks. T, Golgi apparatus next to a normal, tubular-vesicular trans-Golgi network/early endosome (TGN/EE) in a wild-type Columbia-0 (WT) root meristematic cell. S and U, Aberrant TGN/EE composed of several vesicles but no tubular structures (arrowhead in U compared to T) next to a morphologically normal Golgi (g) in *act7-6*. n = 3 5-d-old roots analyzed per genotype. Bars = 10 μm in A to P and 200 nm in S to U.

To test in which subcellular compartments PEN3-GFP accumulates in *exo84b* mutants, we generated *exo84b-1* lines coexpressing PEN3-GFP with SYP32-mCherry/WAVE22R or VHA-a1-mRFP. Quantitative analysis of confocal laser-scanning microscopy (CLSM) images revealed that PEN3-GFP preferentially coaccumulated with the TGN marker VHA-a1-mRFP when compared to SYP32-mCherry/WAVE22R (Fig. 7, I–K).

To examine dynamics of PEN3 polarity establishment, we performed fluorescence recovery after photobleaching

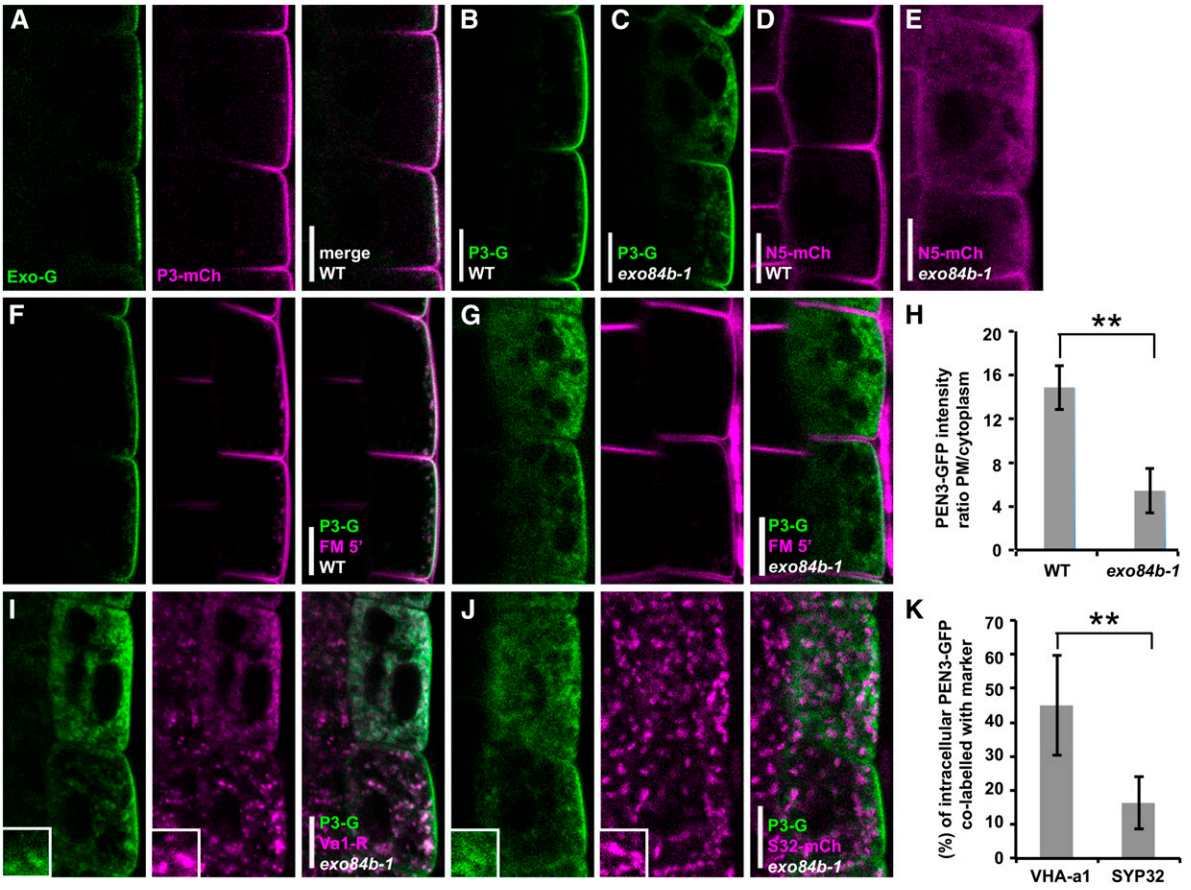

Figure 7. *exo84b* mutants display defective polar outer lateral membrane protein localization with preferential localization to the TGN. A to G, Root epidermal cells of 5-d-old seedlings. A, PEN3-mCherry (P3-mCh, magenta) and EXO84b-GFP (Exo-G) at polar outer lateral PM domain. B, PEN3-GFP (P3-G) in wild type. C, PEN3-GFP (P3-G) in *exo84b-1*. Note, intracellular accumulation of PEN3-GFP and loss of PEN3 polarity in one cell in C. D, NIP5;1-mCherry (N5-mCh) in wild type. E, NIP5;1-mCherry in *exo84b-1*. F and G, Cells expressing PEN3-GFP (P3-G, green) labeled with FM4-64 (FM, magenta) for 5 min in (F) wild type (WT) and (G) *exo84b-1*. (H), Quantification of the lateral PM domain/cytoplasmic PEN3-GFP signal intensity ratio in wild type (WT) and *exo84b-1*. Data are derived from CLSM images such as in F and G. $^{**}P = 0.000$ wild type versus *exo84b-1*, determined by Student's two-tailed *t* test with equal variance, $n = 30$ cells from 15 wild-type roots and from 17 *exo84b-1* roots. I and J, Colocalization analyses in root epidermal cells of 5-d-old *exo84b-1* seedlings coexpressing (I) PEN3-GFP (P3-G, green) and VHA-a1-mRFP (Va1-R, magenta) and (J) P3-G (green) and SYP32-mCherry/WAVE23R (S32-mCh, magenta). K, Quantitative colocalization analysis between intracellular PEN3-GFP and the VHA-a1 or SYP32 markers. Data are derived from CLSM images such as in I and J. $^{**}P = 0.000$ VHA-a1 versus SYP32, determined by Student's two-tailed *t* test with equal variance. Data were average ± SD from $n = 15$ cells per marker. Bars = 10 μm.

(FRAP) analyses by bleaching PEN3-GFP fluorescence at the outer lateral PM and by observing recovery. In wild type, PEN3-GFP displayed polar recovery at the outer lateral PM (Fig. 8A; Supplemental Fig. S4A), while in the *exo84b-1* mutant FRAP of PEN3-GFP was strongly impaired at the outer lateral PM, although recovery was clearly observed in intracellular compartments (Fig. 8B; Supplemental Fig. S4B). We quantified polar recovery by determining the polar index referring to the ratio of signal intensity at the outer lateral versus the inner lateral PM of the cell. The polar index of the wild type (9.95 ± 1.22) proved clearly and significantly higher than the polar index in the *exo84b-1* mutant (6.46 ± 1.50) prior to photobleaching (Fig. 8C). During fluorescence recovery, the polar index increased even 3 h after photobleaching, resulting in polar distribution of PEN3-GFP at the outer lateral PM (Fig. 8C). The *exo84b-1* mutant, however, displayed a much less pronounced increase in polar index compared to the wild type (Fig. 8C), indicating defective polarity establishment. We also analyzed the PM marker EGFP-LTI6a in the *exo84b-1* mutant and observed strong EGFP-LTI6a mislocalization in intracellular compartments of root epidermal cells (Supplemental Figure S5, A and B). When performing FRAP analysis and quantification of polar recovery (Supplemental Figure S5, A–C), we observed that EGFP-LTI6a displayed a slight outer lateral PM polarity (polar index 1.72 ± 0.58) prior to photobleaching, while the polar index in the *exo84b-1* mutant was significantly

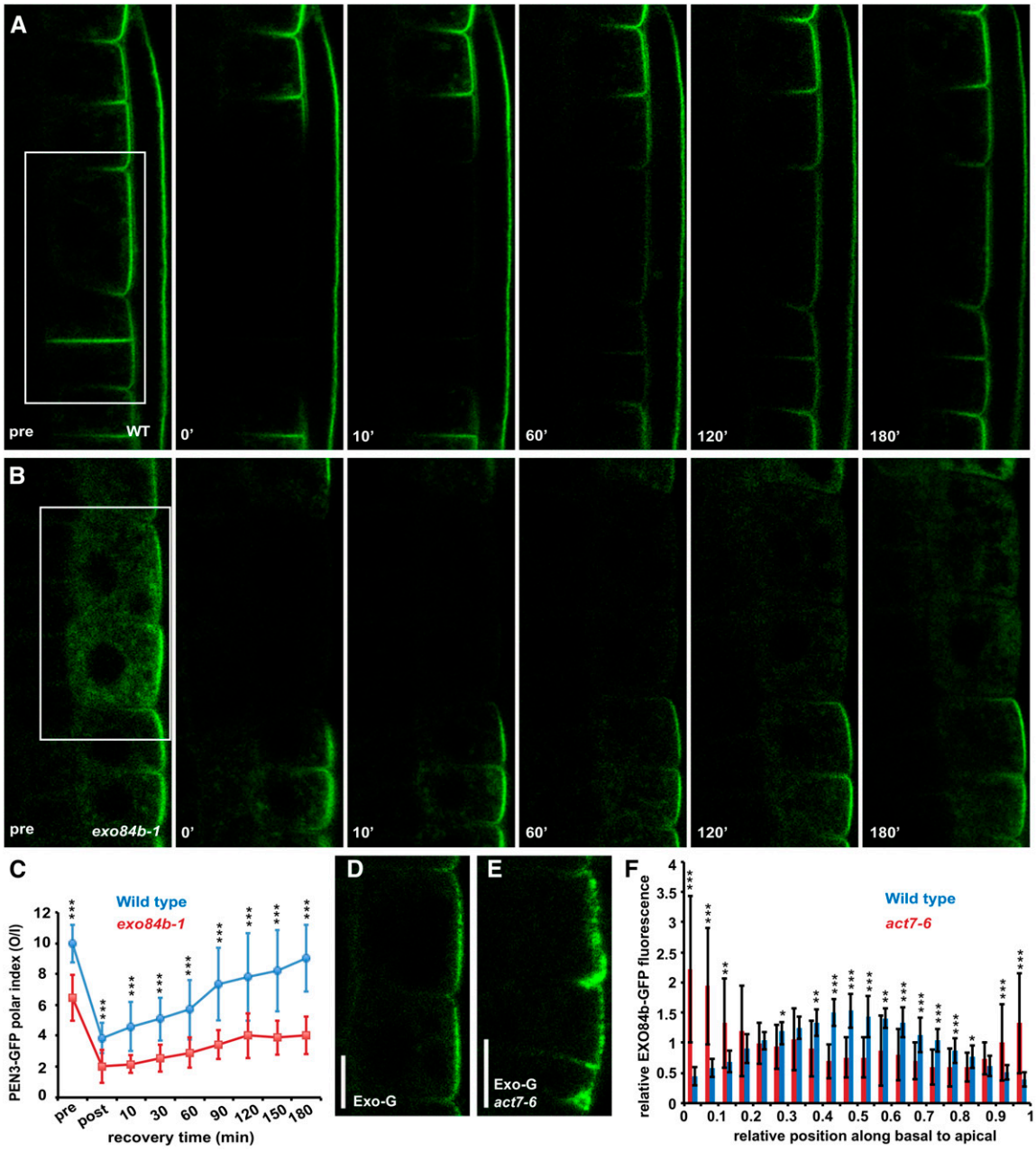

Figure 8. Actin-dependent EXO84b mediates polar PEN3 polarity at the outer lateral membrane. A and B, Representative images of whole-cell FRAP analyses of PEN3-GFP in (A) wild type (WT) and (B) *exo84b-1*. Prebleach images (pre) with a rectangular bleach ROI are indicated. Postbleach time points during fluorescence recovery are indicated in minutes. C, Quantitative analysis of FRAP experiments. ***P = 0.000 wild type versus *exo84b-1*, determined by Student's two-tailed t test with equal variance, n = 13 cells from six wild-type roots, and n = 10 cells from five *exo84b-1* roots. The ratio of intensity of PEN3-GFP fluorescence at the outer lateral PM region to the inner lateral membrane region is indicated as the polar index. Averages and ± SD are indicated with n = 13 and n = 10 for wild type and *exo84b-1*, respectively. EXO84b-GFP localization in (D) wild type, (E) *act7-6* mutant. Note, signal clusters at the outer membrane in E. F, Quantitative analysis of relative EXO84b-GFP fluorescence intensity. Pixel intensity of EXO84b-GFP fluorescence at the outer lateral PM domain was extracted using Fiji software, and the outer membrane was evenly divided into 20 sections from basal to apical. The mean fluorescence intensity of each section was divided by the mean intensity of outer lateral PM domain to obtain the relative fluorescence intensity. Averages and ± SD are indicated with n = 16 cells from six wild-type roots and from seven *act7-6* roots. Student's two-tailed t test with equal variance was employed to detect significances of differences. ***$P < 0.001$, **$P < 0.01$, and *$P < 0.05$. Bars = 10 μm.

reduced to nonpolar distribution (polar index 0.99 ± 0.20; Supplemental Fig. S5C). During fluorescence recovery, the polar index was gradually, slightly increasing in both wild type and *exo84b-1* mutant (Supplemental Fig. S5, C and C′, compared with Fig. 8C). Taken together, our results reveal that EXO84b is required for polarity establishment of proteins at the outer lateral PM domain.

We finally examined the distribution of EXO84b-GFP in *act7-6*, where, in contrast to PEN3-GFP, EXO84b-GFP did not accumulate in intracellular TGN membrane agglomerations but was irregularly distributed along the outer lateral membrane, often accumulating toward the apical or basal ends of this PM domain (Fig. 8, D–F). These findings identify a requirement of ACT7 for correct polar EXO84b distribution at the outer lateral PM.

DISCUSSION

In this study, we reveal a contribution of endocytic recycling to PEN3 outer lateral membrane localization based on photoswitchable protein technology. In contrast to apical and basal cargo trafficking (Geldner et al., 2001, 2003), endocytic recycling had previously remained unnoticed for PEN3 trafficking, which had been investigated under aspects of polar secretion (Łangowski et al., 2010). Our findings demonstrate that both secretory and endocytic PEN3 trafficking utilize the TGN as a main sorting hub for targeting to the polar outer lateral domain. Furthermore, our live imaging analyses reveal that this pathway in vivo utilizes TGN-compartments containing VHA-a1, SYP61, and VTI12. Previous studies suggested actin dependence of PEN3 secretory trafficking based on pharmacological interference (Łangowski et al., 2010). We now demonstrate an additional strong requirement for actin function in PEN3 endocytic recycling and identify ACT7 as a major isoform required for actin-dependent trafficking from the TGN to the PM. The large accumulation of TGN-derived vesicles observed in *act7* mutants appeared strikingly similar to those found in BFA compartments (Grebe et al., 2003), and we observed similar clustering of seemingly intact Golgi stacks around these vesicle agglomerations. Thus, ACT7 function appears to be required for both subcellular Golgi distribution and trafficking of TGN-derived vesicles. In *act7* mutants, these can be observed in large accumulations that are rapidly labeled by the endocytic tracer FM4-64 and accumulate outer lateral cargos such as PEN3 and NIP5;1 in addition to other recently reported PM proteins (Zhu et al., 2016). Since photoswitched PEN3-Eos2 cannot leave these compartments toward the PM, loss of *ACT7* function apparently induces a block at the TGN level along the endocytic recycling pathway. This interpretation was corroborated by BFA washout experiments in presence of LatB. Intriguingly, while polar localization of EXO84b at the outer PM domain protein was perturbed, EXO84b did not accumulate in intracellular compartments of *act7* mutants. This suggests a second independent requirement of ACT7 function for EXO84 polar PM localization. This view is supported by pharmacological interference with actin function (Fendrych et al., 2013). Our study thus reveals two mechanistically different requirements for ACT7 function in trafficking and tethering of outer lateral membrane cargos. PEN3 trafficking and polar localization strongly required EXO84b function. Considering its outer polar localization, we asked whether EXO84b contributes to PEN3 polar tethering and observed strongly reduced polar PM recovery of PEN3-GFP in FRAP studies on the *exo84b* mutant, where PEN3-GFP accumulated cytoplasmically, preferably in TGN compartments. Mislocalization of the second lateral membrane cargo NIP5;1 corroborated both ACT7 and EXO84b function for outer lateral membrane trafficking and polarity establishment, respectively. Our findings reveal that polar tethering of the outer lateral domain cargos PEN3 and NIP5;1 is promoted by EXO84b. The *exo70A1* mutant defective in another component of the exocyst complex displays reduced exit of PIN proteins and of the BASSINOSTEROID INSENSITIVE1 protein from BFA compartments after BFA washout (Drdová et al., 2013). However, neither protein synthesis was blocked nor were PIN or BASSINOSTEROID INSENSITIVE1 cargo proteins traced, for example as a photoswitchable protein fusion in this study (Drdová et al., 2013), and it, therefore, remained difficult to assess whether these cargoes were recycled to the PM. In *Schizosaccharomyces pombe*, the exocyst subunits Sec3 and Exo70 require actin function for their post-Golgi transport (Bendezú et al., 2012), while in *Saccharomyces cerevisiae*, polar Exo84p localization at the budding site depends on Tropomyosin1 and 2 and, thus, likely on actin function (Zhang et al., 2005). Strikingly, the *Drosophila melanogaster* EXO84 homolog mediates embryonic apical epithelial identity (Blankenship et al., 2007). However, cytoskeletal requirements for EXO84 distribution and its polar apical domain localization have not been reported for *D. melanogaster*. Our findings suggest that exocyst-dependent polar tethering mechanisms may have been convergently adopted during apical and outer lateral domain formation in animals and plants, respectively. Moreover, interactions between the actin cytoskeleton and exocyst subunits can occur at different subcellular locations such as at the level of post-Golgi trafficking in yeast and at the PM in Arabidopsis. Our work thus provides an entry for future studies on actin-dependent outer lateral membrane trafficking and polar tethering as well as the molecular mode of interaction between the actin cytoskeleton and the exocyst complex during these processes.

MATERIALS AND METHODS

Plant Materials and Growth Conditions

Arabidopsis (*Arabidopsis thaliana*) ecotype Columbia-0 was used as the wild type. Mutants or marker lines employed in this study were provided by the corresponding authors of cited publications or obtained from the Nottingham Arabidopsis Stock Centre: *act7-6* (N670149; Kiefer et al., 2015), *act7-7* (N447790;

Kiefer et al., 2015), *act2-3* (N6959; Nishimura et al., 2003), *exo84b-1* (Fendrych et al., 2010), *pPEN3:PEN3-GFP pen3-1* (Stein et al., 2006), *pVHA-a1:VHA-a1-mRFP* (Dettmer et al., 2006), *pUBQ10:VTI12-mCherry/WAVE13R* (Geldner et al., 2009), *pUBQ10:SYP32-mCherry/WAVE22R* (Geldner et al., 2009), *pSYP61:SYP61-CFP* (Robert et al., 2008), *pEXO84:EXO84b-GFP exo84b-2* (Fendrych et al., 2010), *p35S:mCherry-TUA5* (Gutierrez et al., 2009; Sampathkumar et al., 2011), *p35S:EGFP-LTI6a* (Grebe et al., 2003), and *p35S:GFP-ABD2-GFP* (Wang et al., 2008). Plant growth conditions were as described previously (Fischer et al., 2006), with minor modifications. In brief, seeds were surface sterilized and stratified at 4°C for 3 d prior to plating on 0.5× Murashige and Skoog (MS) plates (0.5× MS, 1% Suc, 2.5 mM MES [Sigma-Aldrich]). Seedlings were grown vertically at 23°C day and 18°C night under 16-h light/8-h dark photoperiod and subjected to analysis after 5 d.

Inhibitor Treatments

For inhibitor experiments, seedlings were treated in liquid medium (LM) containing 0.5× MS, 1% Suc, 2.5 mM morpholinoethanesulfonic acid (Sigma-Aldrich) at pH 5.8. BFA (Sigma-Aldrich) dissolved in DMSO was used at 50 μM for 1 h or indicated time. CHX (Sigma-Aldrich) was added from a 50 mM aqueous stock to a final concentration of 50 μM. Wm (Sigma-Aldrich) dissolved in DMSO was used at 33 μM for 1 h or indicated times. ConcA (Sigma-Aldrich) was used at 2 μM from a 2-mM stock solution in DMSO. LatB (Sigma-Aldrich) was used at 10 μM from a 10-mM stock solution in DMSO. Jas (Sigma-Aldrich) was applied at 5 μM for 3 h from a 5-mM stock solution in DMSO. Oryzalin (Sigma-Aldrich) was used at 10 μM for 2.5 h from a 100-mM stock solution in DMSO. In control experiments, seedlings mounted in LM containing an equal amount of 0.1% to 0.2% DMSO were observed.

CLSM, Quantitative Image, and Colocalization Analyses

Laser excitation lines for the different fluorophores were 405 nm for CFP, 488 nm for GFP, and 561 nm for mRFP, mCherry, or FM4-64 fluorescence, respectively. Fluorescence emission was detected at 446 to 488 nm for CFP, 492 to 539 nm for GFP, 596 to 650 nm for mRFP or mCherry, 600 to 700 nm for FM4-64 fluorescence. In multilabeling studies, detection was in sequential line-scanning mode with a line average of 4. Live imaging was mostly performed with a Zeiss LSM780 spectral CLSM system equipped with a 32-channel gallium arsenide phosphide detector array mounted on a Zeiss Axio observer Z1 inverted microscope, employing a water-corrected C-Apochromat 40× objective, NA.1.2 (M27; Zeiss) or a Leica TCS SP2 AOBS spectral confocal laser-scanning microscopy system mounted on a Leica DM IRE2 inverted microscope, employing a water-corrected 63× objective NA 1.2 (Leica). Images were analyzed with Fiji software, overlaid in Adobe Photoshop CS5 (Adobe Systems) and assembled in Adobe Illustrator CS5 (Adobe Systems).

Colocalization analyses were performed as described (Boutté et al., 2006; Boutté et al., 2010). In brief, the distance between the geometric centers (centroids) of two labeled objects in two different channels was calculated for each colocalization event. The centroid coordinates were obtained by 3D objects counter function using Fiji software. When the distance between the two centroids of two different channels was below the 250-nm resolution limit of the objective in XY direction, this was scored as one colocalization event. Then the percentage of colabeled objects per optical section was determined.

Quantification of CHX and Wm Effects on BFA Compartment Formation

For quantification of PEN3-GFP agglomeration in BFA compartments, seedlings were either treated with BFA, or with 1 h CHX pretreatment followed by CHX and BFA, or 1 h Wm pretreatment followed by Wm and BFA, or with 1 h CHX plus Wm pretreatment followed by CHX, Wm, and BFA treatment for 60 min. The transition zone of the root epidermis was chosen to take images 60 ± 5 min after treatment from one midplane CLSM section of 20 roots each per treatment employing the same microscope settings. Each image was converted by the image-adjust-threshold function in Fiji software (http://imagej.nih.gov/ij/). Values of area and mean signal intensity for each region of interest (ROI) were obtained employing the area function of Fiji software. Then the intensity in each selected area was obtained by mean signal intensity of the ROI multiplied by area of ROI. Areas larger than 0.5 μm^2 were counted as agglomerations and the number of those was determined per root section. Both concerning the area size of BFA compartments and their relative signal intensity, differences in size, or intensity distributions between treatments were tested for significance by nonparametric Kolmogorov-Smirnov (KS) test (http://www.physics.csbsju.edu/stats/KS-test.n.plot_form.html). For BFA body number per root, a two-tailed unpaired *t* test with equal variance was used to detect statistical differences.

CHX Inhibition Effect of Protein Synthesis

In order to quantify the CHX effect on protein synthesis in ConcA treatment analysis, seedlings were treated with ConcA or CHX 45 min pretreatment followed by CHX with ConcA. Then seedlings were transferred onto slides for observation. The transition zone of the root epidermis was chosen to take images 70 ± 5 min after treatment from one midplane CLSM section from 10 roots for each treatment using the same microscope settings. Values of area and mean signal intensity for each cell (excluding PM) were obtained employing the area function of Fiji software. Subsequently, the intensity in each cell was obtained by mean signal intensity of ROI multiplied by area of ROI. Significant differences were determined by nonparametric KS test (http://www.physics.csbsju.edu/stats/KS-test.n.plot_form.html).

FM4-64 Staining

FM4-64 staining was performed as described (Boutté et al., 2010). Briefly, 5-d-old seedlings were incubated for 5 min on ice in LM containing 25 μM FM4-64 (Molecular Probes), made from a 25 mM stock in DMSO. This was followed by two washes with LM on ice, mounting on coverslips in LM, containing inhibitors as specified, and subsequent observation by CLSM.

Quantification of PEN3-GFP Localization in *exo84b-1* and EXO84b-GFP Localization in *act7-6*

For quantification of PEN3-GFP localization at the outer lateral PM domain and in the cytoplasm, FM4-64 staining was performed to outline the outer lateral PM and CLSM images were obtained within 3 to 10 min after FM4-64 staining. Mean fluorescence intensities of PEN3-GFP at the PM and in the cytoplasm were measured by creating a region of interest covering the whole cytoplasm and the outer lateral PM domain, respectively, in Fiji software and the ratio between the mean intensities was calculated.

For quantification of EXO84b-GFP localization at the outer lateral PM, pixel fluorescence intensity of EXO84b-GFP on the outer lateral PM was extracted using the plot profile function in Fiji software. The outer lateral PM domain was evenly divided into 20 sections from basal to apical, and the mean fluorescence intensity of each section was divided by the mean intensity of the outer lateral PM to obtain the relative fluorescence intensity. Student's two-tailed *t* test with equal variance was employed to assess significances of differences between the distributions.

FRAP Analysis of Fluorescent Fusion Proteins

FRAP experiments were performed as described previously (Men et al., 2008; Boutté et al., 2010; Frescatada-Rosa et al., 2014). In brief, FRAP experiments were performed with a Zeiss LSM 780 confocal laser-scanning system mounted on a Zeiss Axio observer Z1 inverted microscope, employing a water-corrected C-Apochromat 40× objective, numerical aperture 1.2 (Zeiss). Two to three consecutive cells per root were selected for full bleaching. Within these cells, 30 bleaching iterations were performed at five to eight different Z positions and 100% laser power of the 405 nm, 488 nm, and 561 nm laser lines. Pre- and postbleach scans were performed at 2% laser power of the 488 nm laser line, and GFP emission was detected between 488 and 581 nm. Postbleach images were acquired at indicated times using four line averages in line scanning mode with the same microscope settings. In order to quantify polar recovery, fluorescence intensities were measured for both outer and inner membrane regions of bleached cells for pre- and postbleach time points. Fluorescence intensities of nonbleached neighboring cells, as well as background were also determined for all pre- and postbleach time points and these values were used to correct for background fluorescence. To normalize for loss of fluorescence within the bleach and FRAP periods caused by initial photobleaching and excitation during postbleach image acquisition, mean values from the nonbleached neighboring cells were used for correction. Then, the ratio of fluorescence intensity between outer and inner side of bleached cells membrane was calculated as the polar index. A higher ratio indicates the relatively higher reappearance of fluorescence at the outer compared to the inner membrane region.

Photoconversion of PEN3-mEos2 and Quantitative Image Analysis

For photoconversion, a desired ROI was selected and pulsed at 1.5% to 5.5% power of a 405-nm Diode UV laser with 25 bleaching iterations. Green fluorescence of nonconverted mEos2 was excited with a 488 nm Argon-laser line (4% power) and emission detected between 496 and 530 nm. Red fluorescence of the photoconverted mEos2 was excited with 561 nm Diode laser (4% power) and emission detected between 573 and 657 nm. One image was taken prior to photoconversion. Subsequent to photoconversion images were taken at the same photo-multiplier settings at indicated time points.

In order to track PEN3 endocytosis, a selected ROI at the PM was photoconverted. Subsequently, liquid MS medium was replaced with the same medium containing 50 μM BFA to follow BFA compartment formation. The intensity of photoconverted PEN3-mEos2 at outer lateral PM and in BFA compartments was measured at indicated time points by Fiji software.

To track PEN3 recycling to the PM, seedlings were treated with 50 μM BFA for 1 h, and then BFA was washed out with LM in presence or in absence of LatB. Subsequently, a single BFA compartment was photoconverted, and images were taken at indicated time points. The intensity of photoconverted PEN3-mEos2 at the outer lateral PM after BFA washout in presence or absence of LatB was measured by employing Fiji software. The intensity of PEN3-Eos-R fluorescence at PM after 30 min or 60 min BFA washout (I_{tx}) divided by the respective PM intensity immediately after photoconversion (I_{t0}) was calculated as PEN3-Eos-R PM intensity ratio relative to t0 (I_{tx}/I_{t0}). Here, I_{tx} refers to the intensity of red photoconverted PEN3-mEos2 at the outer lateral PM 30 min or 60 min after BFA washout in presence or in absence of LatB. I_{t0} refers to the respective photoconverted PEN3-mEos2 red-fluorescence intensity at the outer lateral PM just after BFA washout and subsequent photoconversion of PEN3-mEos2 in the BFA compartment.

To track PEN3-mEos2 redistribution from ACT7-compartments to the PM in *act7-6*, the intensities of photoconverted PEN3-mEos2 at the outer layer PM and in ACT7 compartments were determined at indicated time points by employing Fiji software.

The intensity from the region of a neighboring cell not expressing PEN3-mEos2 was also measured to correct for background fluorescence for each experiment. All data were box-plotted employing Excel software (version 14.4.5, Microsoft Corporation). For each data set minimum value (lower whisker), lower quartile (green box), median value, upper quartile (violet box), and maximum value (upper whisker) of the population are displayed. Statistical differences between different time points were determined by two-tailed, type 1 paired *t* test.

Transmission Electron Microscopy

Root tips from 5-d-old Arabidopsis seedlings were submerged in freezing medium (200 mM Suc, 10 mM trehalose, 10 mM Tris buffer, pH 6.6), transferred into planchettes (Leica Microsystems; 3.0 × 0.5 mm, Al, type A and B), and frozen in a high-pressure freezer HPM100 (Leica Microsystems). Freeze substitution was performed in a Leica EM AFS2 freeze substitution unit (Leica Microsystems) in dry acetone supplemented with 0.4% uranyl acetate at −85°C for 36 h, followed by 5 h warm-up to −50°C. After washing with 100% ethanol for 60 min, the roots were infiltrated and embedded in Lowicryl HM20 resin at −50°C (intermediate steps with 30%, 50%, and 70% HM20 in ethanol, 1 h each) and polymerized for 3 d with ultraviolet light in the freeze substitution apparatus. Ultrathin sections were cut on a Leica Ultracut UCT ultramicrotome, poststained with aqueous uranyl acetate/lead citrate and examined in a CM100 (Philips) transmission electron microscope operating at 100 kV. Negatives (MACO EM films TYP S, 6.5 × 9 cm, ES 206) were scanned with a 9000F Mark II system (Canon).

Plasmid Construction and Plant Transformation

To generate a PEN3 fusion to mEos2, two PCRs were initially performed to amplify two overlapping fragments including 2502 bp upstream and 5181 bp downstream of the ATG of the *PEN3* gene with primer pairs *Eco*RIPEN3F2, 5′-gaattcATTAGAGCTCGAAACTGAGATGGA-3′and HalfXbaIR, 5′-CCATGAAGAGTGTCTTAGTAGGTCCA-3′; HalfXbaIF, 5′-TCTCAAAG-TGAGTCCAACTCTCGCCT-3′ and *Bam*HIPEN3R1, 5′-ggatccTCTGGTCTG-GAAGTTGAGAGTTCTGA-3′, respectively. The two fragments were ligated at the overlapping *Xba*I site located 1252 bp downstream of the ATG to obtain a DNA fragment including promoter and coding region of *PEN3*, and the resulting insert was named *PEN3PC*. *PEN3PC* was subcloned into pGREENII0029 (John Innes Centre; Hellens et al., 2000) via *Eco*RI and *Bam*HI. Moreover, 2739 bp downstream of the stop codon were amplified as the 3′UTR of *PEN3* employing forward primer *Sal*IPEN3F3, 5′-gtcgacAACCATCTCTCAAACAA-CAAAGTCTCT-3′ and reverse primer 3UTRPEN3R2, 5′-GGTAAGTA-GAGCAAACGATTCGGCT-3′. The resulting fragment was subcloned into pBluescript SKII by blunt-end ligation at the *Sma*I site. The coding sequence of mEos2 (McKinney et al., 2009) was amplified from Addgene plasmid 20341, pRSETa mEos2 (https://www.addgene.org/20341/), employing primers *Bam*-HIEOS2F3, 5′-GGATCCGCTGCTGCCGCTGCCGCTGCGGCAGCGGCCG-GACCGGTCGCCACCATGAGTGCGATTAAGCCAGACATGAAGA-3′ and *Sal*IEos2R2, 5′-ttgtcgacTTATCGTCTGGCATTGTCAGGCAATCC-3′. In this way, 15 amino acids serving as a linker between PEN3 and mEos2 were added prior to the ATG of mEos2. The resulting fragment was also subcloned into pBluescript SKII. Finally, PEN3PC in pGREENII0029 was digested by *Eco*RI and *Bam*HI, mEos2 in pBluescript SKII was digested by *Bam*HI and *Sal*I, and the 3′UTR in pBluescript SKII was digested by *Sal*I and *Kpn*I. These three fragments were concomitantly ligated into pGREENII0029 digested by *Eco*RI and *Kpn*I. The same procedure was used to generate the PEN3-mCherry fusion, but without inserting a linker between PEN3 and mCherry.

To generate an H2B fusion to mCherry, the vector pGreenII0179 (John Innes Centre, Norwich, UK; Hellens et al., 2000) was digested with *Kpn*I and *Sac*I to remove the multiple cloning site, and both 5′ and 3′ overhangs were blunted for blunt-end ligation. A 35S-CaMV cassette (John Innes Centre; Hellens et al., 2000), including a CaMV 35S promoter and a CaMV terminator derived from vector p35S-2 (John Innes Centre; Hellens et al., 2000) was excised with *Eco*RV and cloned into the blunted pGreenII0179 vector (John Innes Centre; Hellens et al., 2000) generating pGreenII0179_35S-CaMV. An Arabidopsis *HISTONE2B* cDNA fragment followed by the sequence encoding for a poly-Ala linker and the *Venus* coding sequence was synthesized with *Xba*I and *Eco*RI sites (Genscript) and cloned into pGreenII0179_35S-CaMV via *Xba*I and *Eco*RI giving rise to pGreenII0179_35S::H2B-Venus. An mCherry fragment with poly-Ala linker was amplified by PCR from synthesized mCherry-LTI6a cloned into pUC57 (Genscript), employing forward primer H2B_Cherry_F, 5′-GCGGCCGCTGCCGCTGCGGCAGCGGCCatggt-gagcaagggcgagg-3′ and reverse primer H2B_Cherry_R, 5′-TTACTTGTA-CAGCTCGTCCATGC-3′, and subcloned into pBluescriptII SK(-) (Stratagene). To obtain the H2B fused to mCherry, the region of Venus in pGreenII0179_35S:: H2B-Venus was replaced with mCherry with *Not*I and *Bsr*GI (pGree-nII0179_35S::H2B-mCherry).

Phusion DNA polymerase (Thermo Fisher Scientific) was used in all PCR reactions. Restriction enzymes were purchased from Fermentas (Thermo Fisher Scientific). Synthetic oligonucleotides were obtained from MWG (MWG, Biotech AG). Plasmid constructs were sequenced by MWG and introduced into *Agrobacterium tumefaciens* GV3101, which were used to transform Arabidopsis Columbia-0 by floral dipping (Clough and Bent, 1998).

Genetic Screen for Subcellular PEN3-GFP Mislocalization

Plasmid pGreenII0179_35S::H2B-mCherry was transformed into *Agrobacterium tumefaciens* strain GV3101 and introduced into *pPEN3:PEN3-GFP; pen3-1* (Stein et al., 2006) employing the floral dip method (Clough and Bent, 1998). Transgenic plants were selected based on resistance to 20 μg/ml hygromycin (Duchefa Biochemie). A T4 line homozygous for both transgenes and stably expressing both the PEN3-GFP and the H2B-mCherry fusion proteins with no abnormality in localization was chosen for mutagenesis. More than 8,000 T4 seeds were immersed in 0.3% (v/v) ethyl methanesulfonate (Sigma-Aldrich) in sterile ddH_2O for 12 h at room temperature, followed by eight washes with sterile ddH_2O. The resulting M1 seeds were immediately surface sterilized and plated on MS plates. M1 seedlings were vertically grown on MS plates for more than 5 d under growth condition described above and transferred to soil. Seeds were independently harvested from 8,000 individual M1 plants. About 1200 independent M2 lines were screened for mislocalization of PEN3-GFP. To this end, about 30 seedlings of each independent M2 line (about 36,000 M2 seedlings in total) were examined using a Leica TCS SP2 AOBS spectral confocal laser scanning system. *act7-8*, *act7-9*, and *act7-10* were isolated as lines displaying aberrant localization of PEN3-GFP. As the overall seedling morphology of these mutants resembled *act7*, *act7-8* was crossed to *act7-6*, which failed to complement the PEN3-GFP mislocalization phenotype in the F1, indicating allelelism. The coding sequence of ACT7 was amplified and sequenced revealing the above-described mutations. Further analyses were performed in the *act7-6* T-DNA insertion mutant background characterized previously (Kiefer et al., 2015).

Accession Numbers

Sequence data from this article can be found in the Arabidopsis Genome Initiative or GenBank/EMBL databases under the following accession numbers: *PEN3* (At1g59870), *VHA-a1* (At2g28520), *SYP61* (At1g28490), *SYP32* (At3g24350), *ACT2* (At3g18780), *ACT7* (At5g09810), *EXO84b* (At5g49830), *VTI12* (At1g26670), *H2B* (At5g22880), and *TUA5* (At5g19780).

Supplemental Data

The following supplemental materials are available.

Supplemental Figure S1. Complementation of the *pen3-4* long-root-hair phenotype.

Supplemental Figure S2. Contributions of the actin and tubulin cytoskeletons to outer lateral membrane protein trafficking.

Supplemental Figure S3. *ACT7* is required for trafficking of PM proteins, including outer lateral membrane domain proteins.

Supplemental Figure S4. Whole-cell FRAP analyses of PEN3-GFP in wild-type and *exo84b-1* cells (additional data points).

Supplemental Figure S5. EXO84b mediates EGFP-LTI6a localization at the plasma membrane.

Supplemental Table S1. Significant differences between the average number of BFA bodies per root.

Supplemental Table S2. Significant differences between BFA body size or fluorescence intensity per BFA body among treatments.

Supplemental Movie S1. PEN3-GFP in *exo84b-1* in green channel.

Supplemental Movie S2. PEN3-GFP in *exo84b-1* in gray channel.

ACKNOWLEDGMENTS

We thank David Ehrhardt, Niko Geldner, Natasha Raikhel, Staffan Persson, Karin Schumacher, Shauna Somerville, and Viktor Žárský for sharing published materials. We thank the Nottingham Arabidopsis Stock Centre for providing seed stocks. We thank Jürgen Hartmann at the Max Planck Institute of Colloids and Interfaces, Potsdam-Golm, Germany, for providing access to high-pressure freezing equipment for sample preparation for electron microscopy as well as Stefano Pietra and Michael Sauer for critical reading of the manuscript.

Received August 9, 2016; accepted October 31, 2016; published November 1, 2016.

LITERATURE CITED

Alassimone J, Naseer S, Geldner N (2010) A developmental framework for endodermal differentiation and polarity. Proc Natl Acad Sci USA **107:** 5214–5219

Barberon M, Dubeaux G, Kolb C, Isono E, Zelazny E, Vert G (2014) Polarization of IRON-REGULATED TRANSPORTER 1 (IRT1) to the plant-soil interface plays crucial role in metal homeostasis. Proc Natl Acad Sci USA **111:** 8293–8298

Bendezú FO, Vincenzetti V, Martin SG (2012) Fission yeast Sec3 and Exo70 are transported on actin cables and localize the exocyst complex to cell poles. PLoS One **7:** e40248

Blankenship JT, Fuller MT, Zallen JA (2007) The Drosophila homolog of the Exo84 exocyst subunit promotes apical epithelial identity. J Cell Sci **120:** 3099–3110

Blilou I, Xu J, Wildwater M, Willemsen V, Paponov I, Friml J, Heidstra R, Aida M, Palme K, Scheres B (2005) The PIN auxin efflux facilitator network controls growth and patterning in Arabidopsis roots. Nature **433:** 39–44

Boutté Y, Crosnier MT, Carraro N, Traas J, Satiat-Jeunemaitre B (2006) The plasma membrane recycling pathway and cell polarity in plants: studies on PIN proteins. J Cell Sci **119:** 1255–1265

Boutté Y, Frescatada-Rosa M, Men S, Chow CM, Ebine K, Gustavsson A, Johansson L, Ueda T, Moore I, Jürgens G, et al (2010) Endocytosis restricts Arabidopsis KNOLLE syntaxin to the cell division plane during late cytokinesis. EMBO J **29:** 546–558

Clough SJ, Bent AF (1998) Floral dip: a simplified method for Agrobacterium-mediated transformation of Arabidopsis thaliana. Plant J **16:** 735–743

Dettmer J, Hong-Hermesdorf A, Stierhof YD, Schumacher K (2006) Vacuolar H+-ATPase activity is required for endocytic and secretory trafficking in Arabidopsis. Plant Cell **18:** 715–730

Drakakaki G, van de Ven W, Pan S, Miao Y, Wang J, Keinath NF, Weatherly B, Jiang L, Schumacher K, Hicks G, et al (2012) Isolation and proteomic analysis of the SYP61 compartment reveal its role in exocytic trafficking in Arabidopsis. Cell Res **22:** 413–424

Drdová EJ, Synek L, Pečenková T, Hála M, Kulich I, Fowler JE, Murphy AS, Zárský V (2013) The exocyst complex contributes to PIN auxin efflux carrier recycling and polar auxin transport in Arabidopsis. Plant J **73:** 709–719

Dröse S, Bindseil KU, Bowman EJ, Siebers A, Zeeck A, Altendorf K (1993) Inhibitory effect of modified bafilomycins and concanamycins on P- and V-type adenosinetriphosphatases. Biochemistry **32:** 3902–3906

Emans N, Zimmermann S, Fischer R (2002) Uptake of a fluorescent marker in plant cells is sensitive to brefeldin A and wortmannin. Plant Cell **14:** 71–86

Fendrych M, Synek L, Pecenková T, Drdová EJ, Sekeres J, de Rycke R, Nowack MK, Zársky V (2013) Visualization of the exocyst complex dynamics at the plasma membrane of Arabidopsis thaliana. Mol Biol Cell **24:** 510–520

Fendrych M, Synek L, Pecenková T, Toupalová H, Cole R, Drdová E, Nebesárová J, Sedinová M, Hála M, Fowler JE, et al (2010) The Arabidopsis exocyst complex is involved in cytokinesis and cell plate maturation. Plant Cell **22:** 3053–3065

Frescatada-Rosa M, Stanislas T, Backues SK, Reichardt I, Men S, Boutté Y, Jürgens G, Moritz T, Bednarek SY, Grebe M (2014) High lipid order of Arabidopsis cell-plate membranes mediated by sterol and DYNAMIN-RELATED PROTEIN1A function. Plant J **80:** 745–757

Fischer U, Ikeda Y, Ljung K, Serralbo O, Singh M, Heidstra R, Palme K, Scheres B, Grebe M (2006) Vectorial information for Arabidopsis planar polarity is mediated by combined AUX1, EIN2, and GNOM activity. Curr Biol **16:** 2143–2149

Gälweiler L, Guan C, Müller A, Wisman E, Mendgen K, Yephremov A, Palme K (1998) Regulation of polar auxin transport by AtPIN1 in Arabidopsis vascular tissue. Science **282:** 2226–2230

Geldner N, Anders N, Wolters H, Keicher J, Kornberger W, Müller P, Delbarre A, Ueda T, Nakano A, Jürgens G (2003) The Arabidopsis GNOM ARF-GEF mediates endosomal recycling, auxin transport, and auxin-dependent plant growth. Cell **112:** 219–230

Geldner N, Dénervaud-Tendon V, Hyman DL, Mayer U, Stierhof YD, Chory J (2009) Rapid, combinatorial analysis of membrane compartments in intact plants with a multicolor marker set. Plant J **59:** 169–178

Geldner N, Friml J, Stierhof YD, Jürgens G, Palme K (2001) Auxin transport inhibitors block PIN1 cycling and vesicle trafficking. Nature **413:** 425–428

Grebe M, Friml J, Swarup R, Ljung K, Sandberg G, Terlou M, Palme K, Bennett MJ, Scheres B (2002) Cell polarity signaling in Arabidopsis involves a BFA-sensitive auxin influx pathway. Curr Biol **12:** 329–334

Grebe M, Xu J, Möbius W, Ueda T, Nakano A, Geuze HJ, Rook MB, Scheres B (2003) Arabidopsis sterol endocytosis involves actin-mediated trafficking via ARA6-positive early endosomes. Curr Biol **13:** 1378–1387

Gutierrez R, Lindeboom JJ, Paredez AR, Emons AM, Ehrhardt DW (2009) Arabidopsis cortical microtubules position cellulose synthase delivery to the plasma membrane and interact with cellulose synthase trafficking compartments. Nat Cell Biol **11:** 797–806

Heider MR, Munson M (2012) Exorcising the exocyst complex. Traffic **13:** 898–907

Hellens RP, Edwards EA, Leyland NR, Bean S, Mullineaux PM (2000) pGreen: a versatile and flexible binary Ti vector for Agrobacterium-mediated plant transformation. Plant Mol Biol **42:** 819–832

Ikeda Y, Men S, Fischer U, Stepanova AN, Alonso JM, Ljung K, Grebe M (2009) Local auxin biosynthesis modulates gradient-directed planar polarity in Arabidopsis. Nat Cell Biol **11:** 731–738

Jaillais Y, Fobis-Loisy I, Miège C, Rollin C, Gaude T (2006) AtSNX1 defines an endosome for auxin-carrier trafficking in Arabidopsis. Nature **443:** 106–109

Kiefer CS, Claes AR, Nzayisenga JC, Pietra S, Stanislas T, Hüser A, Ikeda Y, Grebe M (2015) Arabidopsis AIP1-2 restricted by WER-mediated patterning modulates planar polarity. Development **142:** 151–161

Kleine-Vehn J, Friml J (2008) Polar targeting and endocytic recycling in auxin-dependent plant development. Annu Rev Cell Dev Biol **24:** 447–473

Łangowski L, Růzicka K, Naramoto S, Kleine-Vehn J, Friml J (2010) Trafficking to the outer polar domain defines the root-soil interface. Curr Biol **20:** 904–908

McKinney SA, Murphy CS, Hazelwood KL, Davidson MW, Looger LL (2009) A bright and photostable photoconvertible fluorescent protein. Nat Methods **6:** 131–133

Men S, Boutté Y, Ikeda Y, Li X, Palme K, Stierhof YD, Hartmann MA, Moritz T, Grebe M (2008) Sterol-dependent endocytosis mediates post-cytokinetic acquisition of PIN2 auxin efflux carrier polarity. Nat Cell Biol **10:** 237–244

Michniewicz M, Zago MK, Abas L, Weijers D, Schweighofer A, Meskiene I, Heisler MG, Ohno C, Zhang J, Huang F, et al (2007) Antagonistic regulation of PIN phosphorylation by PP2A and PINOID directs auxin flux. Cell **130:** 1044–1056

Miwa K, Takano J, Omori H, Seki M, Shinozaki K, Fujiwara T (2007) Plants tolerant of high boron levels. Science **318:** 1417

Müller A, Guan C, Gälweiler L, Tänzler P, Huijser P, Marchant A, Parry G, Bennett M, Wisman E, Palme K (1998) AtPIN2 defines a locus of Arabidopsis for root gravitropism control. EMBO J **17:** 6903–6911

Nishimura T, Yokota E, Wada T, Shimmen T, Okada K (2003) An Arabidopsis ACT2 dominant-negative mutation, which disturbs F-actin polymerization, reveals its distinctive function in root development. Plant Cell Physiol **44:** 1131–1140

Richter S, Geldner N, Schrader J, Wolters H, Stierhof YD, Rios G, Koncz C, Robinson DG, Jürgens G (2007) Functional diversification of closely related ARF-GEFs in protein secretion and recycling. Nature **448:** 488–492

Robert S, Chary SN, Drakakaki G, Li S, Yang Z, Raikhel NV, Hicks GR (2008) Endosidin1 defines a compartment involved in endocytosis of the brassinosteroid receptor BRI1 and the auxin transporters PIN2 and AUX1. Proc Natl Acad Sci USA **105:** 8464–8469

Robineau S, Chabre M, Antonny B (2000) Binding site of brefeldin A at the interface between the small G protein ADP-ribosylation factor 1 (ARF1) and the nucleotide-exchange factor Sec7 domain. Proc Natl Acad Sci USA **97:** 9913–9918

Ruzicka K, Strader LC, Bailly A, Yang H, Blakeslee J, Langowski L, Nejedlá E, Fujita H, Itoh H, Syono K, et al (2010) Arabidopsis PIS1 encodes the ABCG37 transporter of auxinic compounds including the auxin precursor indole-3-butyric acid. Proc Natl Acad Sci USA **107:** 10749–10753

Sampathkumar A, Lindeboom JJ, Debolt S, Gutierrez R, Ehrhardt DW, Ketelaar T, Persson S (2011) Live cell imaging reveals structural associations between the actin and microtubule cytoskeleton in Arabidopsis. Plant Cell **23:** 2302–2313

Stein M, Dittgen J, Sánchez-Rodríguez C, Hou BH, Molina A, Schulze-Lefert P, Lipka V, Somerville S (2006) Arabidopsis PEN3/PDR8, an ATP binding cassette transporter, contributes to nonhost resistance to inappropriate pathogens that enter by direct penetration. Plant Cell **18:** 731–746

Steinmann T, Geldner N, Grebe M, Mangold S, Jackson CL, Paris S, Gälweiler L, Palme K, Jürgens G (1999) Coordinated polar localization of auxin efflux carrier PIN1 by GNOM ARF GEF. Science **286:** 316–318

Strader LC, Bartel B (2009) The Arabidopsis PLEIOTROPIC DRUG RESISTANCE8/ABCG36 ATP binding cassette transporter modulates sensitivity to the auxin precursor indole-3-butyric acid. Plant Cell **21:** 1992–2007

Takano J, Tanaka M, Toyoda A, Miwa K, Kasai K, Fuji K, Onouchi H, Naito S, Fujiwara T (2010) Polar localization and degradation of Arabidopsis boron transporters through distinct trafficking pathways. Proc Natl Acad Sci USA **107:** 5220–5225

Uehara M, Wang S, Kamiya T, Shigenobu S, Yamaguchi K, Fujiwara T, Naito S, Takano J (2014) Identification and characterization of an Arabidopsis mutant with altered localization of NIP5;1, a plasma membrane boric acid channel, reveals the requirement for D-galactose in endomembrane organization. Plant Cell Physiol **55:** 704–714

Underwood W, Somerville SC (2013) Perception of conserved pathogen elicitors at the plasma membrane leads to relocalization of the Arabidopsis PEN3 transporter. Proc Natl Acad Sci USA **110:** 12492–12497

Vida TA, Emr SD (1995) A new vital stain for visualizing vacuolar membrane dynamics and endocytosis in yeast. J Cell Biol **128:** 779–792

Volinia S, Dhand R, Vanhaesebroeck B, MacDougall LK, Stein R, Zvelebil MJ, Domin J, Panaretou C, Waterfield MD (1995) A human phosphatidylinositol 3-kinase complex related to the yeast Vps34p-Vps15p protein sorting system. EMBO J **14:** 3339–3348

Wang YS, Yoo CM, Blancaflor EB (2008) Improved imaging of actin filaments in transgenic Arabidopsis plants expressing a green fluorescent protein fusion to the C- and N-termini of the fimbrin actin-binding domain 2. New Phytol **177:** 525–536

Wisniewska J, Xu J, Seifertová D, Brewer PB, Ruzicka K, Blilou I, Rouquié D, Benková E, Scheres B, Friml J (2006) Polar PIN localization directs auxin flow in plants. Science **312:** 883

Zhang X, Zajac A, Zhang J, Wang P, Li M, Murray J, TerBush D, Guo W (2005) The critical role of Exo84p in the organization and polarized localization of the exocyst complex. J Biol Chem **280:** 20356–20364

Zhu J, Bailly A, Zwiewka M, Sovero V, Di Donato M, Ge P, Oehri J, Aryal B, Hao P, Linnert M, et al (2016) TWISTED DWARF1 mediates the action of auxin transport inhibitors on actin cytoskeleton dynamics. Plant Cell **28:** 930–948